Finite-Temperature Green's Function Methods for ab-initio Quantum Chemistry: Thermodynamics, Spectra, and Quantum Embedding

by

Alicia Rae Welden

A dissertation submitted in partial fulfillment
of the requirements for the degree of
Doctor of Philosophy
(Chemistry)
in the University of Michigan
2018

Doctoral Committee:

Assistant Professor Dominika Zgid, Chair
Professor Eitan Geva
Professor Kevin Kubarych
Associate Professor Vanessa Sih

Alicia Rae Welden
welden@umich.edu
ORCID iD: 0000-0002-2238-9825

DEDICATION

To B.

ACKNOWLEDGMENTS

I am thankful to my advisor Dr. Dominika Zgid, for guiding me through my Ph.D. and believing in me (even if I didn't believe in me). She continued to be supportive and nurturing throughout my graduate school years, and truely shaped me as a person and a scientist.

I would like to thank Dr. Eitan Geva for serving on my committee and for being the advisor of the work we did together on Compute-to-Learn. That project was an excellent opportunity for me to develop as a teacher, and I am grateful for the time he spent advising it, and the opportunities it gave me.

I would like to thank Dr. Kevin Kubarych and Dr. Vanessa Sih for serving on my committee and their helpful guidance during my Ph.D. work.

I am thankful to Blair Winograd for being my colleague and friend. I would not have been able to navigate graduate school without you.

I am thankful to Dr. Alexander Rusakov for being my deskmate, coauthor, and colleague. I would like to acknowledge my group mates Dr. Alexei Kananenka, Dr. Tran Nguyen Lan, Dr. Avijit Shee, and Yanbing Zhou for the opportunity to work and discuss science together. I would like to thank my former group member, Dr. Jordan Phillips, for his patience and for advising me during my first project in graduate school.

I would not be where I am today if it were not for the love and support of my parents, Shirley Reynolds-Pincus and Rick Pincus, who have always encouraged me to do what makes me happy.

I have made many new friends in Michigan and would like to thank them all for the warm and welcoming atmosphere they have created. I would like to thank my non-human supporters, Sterling, Mallory, and Romeo for injecting much cuteness into many of my days.

Last but not at all least, I am thankful for my husband, Brian, and his love, support, and encouragement. Brian, I love you and would not have been able to do this without you.

This thesis was advised by Dr. Dominika Zgid and completed in collaboration with members of my group and the Emanuel Gull's group in the Department of Physics at the University of Michigan. Chapter 3 investigates the ability to obtain temperature dependent electronic thermodynamics from a Green's function and co-authored with Dr. Alexander Rusakov. Chapter 4 describes different ways to obtain the spectra from a temperature-dependent Green's function and was co-authored by Dr. Jordan J. Phillips and Dr. Tran Nyugen Lan. Chapter 5 demonstrates the use of a temperature-dependent restricted active space configuration interaction impurity solver for quantum embedding, and was co-authored with Dr. Sergei Iskakov.

PREFACE

"But the computers have bad features. The main one is that students get so fascinated with them, so immersed with what they can do, that they never get away from the computer far enough to think about what they are doing. This in a way is probably what has kept the chemists from thinking beyond the LCAO method. Ever since they started with computers, they have been using this method, enlarging it more and more, using bigger and bigger computers, without stopping to ask whether there might not be some quite different approach to the problem."

-John C. Slater, 1975

"A thesis is not completed, but merely abandoned."

-Unknown

TABLE OF CONTENTS

LIST OF FIGURES

LIST OF TABLES

ABSTRACT

Description of electron correlation is crucial to chemical accuracy in quantum chemical calculations. However, the interaction of electrons in a system is an insoluble many-body problem. Constructing approximations to describe electron correlation is a challenging task, but there has been success in the quantum chemistry community using wavefunction methods and density functional theory. However, there are still challenges to be overcome in areas such as theoretical solid state chemistry, which requires description of large systems and the use of finite temperature. Large system sizes and finite temperature can be difficult to treat solely with the currently available methods. Therefore, a new class of methods, based on the temperature-dependent Green's function, is implemented and explored.

This thesis is toward investigating the use of temperature-dependent Green's functions for ab-initio quantum chemistry. That is, we are treating a quantum chemical Hamiltonian with realistic electron interactions. While this formalism has been applied to model systems in the condensed matter community, its has been used much less by the quantum chemistry community. Therefore, the numerical behavior and accuracy of Green's function methods for quantum chemical calculations is relatively unknown.

This work investigates the ability of the temperature-dependent Green's function, which is an ensemble formalism, to give access to temperature dependent thermodynamic quantities such as free energy and entropy when calculated in a second-order and perturbative manner (GF2). We find that this method is able to give good accuracy for lower temperatures and excellent accuracy for higher temperatures for a molecular case

and is able to qualitatively describe a simple model of a solid. The results of this work are presented in chapter 3.

Although Green's functions have a clear connection with spectra at zero temperature, it is not straight forward to obtain spectra from the finite temperature Green's function, which is calculated on the imaginary frequency axis. Therefore, we must investigate methods to obtain spectral quantities in a consistent and reliable manner from the imaginary axis. Chapter 4 investigates several methods to do so and we compare our results with experimental and highly accurate benchmark data. We find that it is possible to obtain spectral quantities that can differ by several electron volts, even if the same level of theory is used to obtain the Green's function. This reiterates that finding a spectrum from the imaginary axis is nontrivial and that one must exercise caution when comparing spectral quantities that were calculated using different techniques, even if they are treated with the same theoretical accuracy.

Accessing larger systems with the Green's function requires the use of quantum embedding. Quantum embedding describes nontrivial electron interaction between a highly accurate "active space" or "impurity" and a larger, lower level "environment". It is challenging to construct an impurity solver that is reliable at low temperatures. In chapter 5 of this work, we implement and test a temperature dependent configuration interaction impurity solver for quantum embedding. This solver can be used in quantum embedding schemes such as dynamical mean field theory and self-energy embedding theory for larger systems.

Overall, this thesis has made progress toward using Green's functions for ab-initio quantum chemistry at finite temperature. Groundwork has been laid for using this formalism to calculate thermodynamics and spectra using a Green's function with realistic electron interactions and to explore quantum embedding using an impurity solver at low temperatures.

CHAPTER 1

Introduction

Theoretical chemistry can provide insights to experiments where details at the atomistic level can not be resolved; In particular, one wishes to describe the complex motion of the electrons in a system, i.e., the electron *correlation*. This electron correlation is responsible for much of the interesting chemistry of atoms, molecules, and materials, but is not always straightforward to study through experiment alone. Unfortunately, it is not possible to calculate electron correlation for realistic systems exactly from an analytic theory, requiring approximations to be made. For decades, approximations have been introduced into electronic structure theories that have been translated into computational methods. These methods have provided invaluable insight into many chemical phenomena, and great efforts have been given in the last decades to expanding their use in chemistry.

As quantum chemistry methods were initially developed, computing power required that the first systems calculated were quite small. The first quantitative calculations for many-electron systems were carried out by Hartree and Hartree in 1928 on atomic systems. Eventually, as computing power increased, the number of electrons that could be treated grew, leading to the study of many atoms and molecules of chemical interest. The limitations of computing power and the focus of chemists on molecular systems led to many quantum chemical methods being developed primarily with applications to molecular systems as the ultimate goal. Wavefunction methods such as coupled cluster (CC) and configuration interaction (CI) are used to obtain high accuracy for relatively small numbers of electrons. Using conventional implementations, CC and CI are not capable of

computing more than tens of atoms. Density functional theory (DFT) is a workhorse of electronic structure, and is able to treat relatively large systems by minimizing energy with respect to the ground state electron density. DFT is able to treat hundreds of atoms with a moderate basis. Many of these methods appear in popular software packages and are used routinely by experimental and theoretical chemists.

Simultaneously with the development of quantum chemical methods, solid state theories were explored, which described electronic band structure in solids. Often, electrons were described as independent from each other in a uniform background of positive charges, and this was capable of qualitatively describing many solid state systems. However, this picture begins to break down when electron interactions become non-negligable. For example, NiO is predicted to be a conductor by band theory, because it has a partially filled 3d shell. However, due to the correlation between the d electrons, NiO is actually an insulator. Mean field theories and independent electron models are inadequate to describe systems with localized electrons, and more sophisticated descriptions of the correlation effects must be included.

The field of solid state chemistry is growing, but existing quantum chemical methods are limited in their ability to be applied to solids. Additionally, many solid state theories are only suitable for model systems and are not capable of being applied generally to chemical problems. A new approach to address the specific challenges of modeling solids from a quantum chemical perspective must be developed and investigated.

There are several challenges that need to be overcome in order to do so. The most salient issues that require attention in this area are how to overcome the limitations of the system size that needs to be considered, as well as the inclusion of many excited states, further enlarging the size of the problem. While a molecule can be comprised of several to a few hundred atoms, solids contain of the order of thousands atoms! Consequently, treatment of a solid with a high level quantum chemistry method is well beyond the computational ability of any modern computer, requiring a new set of tools that treat the system efficiently with the available computing resources. In addition to the enormous system size, modeling some solids realistically requires the inclusion of temperature,

increasing the computational cost even further. Most theoretical methods for molecules carry out the calculation at zero temperature, which is a valid description because of the large gap between electronic states. However, solids with small or no gap between electronic states, such as semiconductors and metals, have states occupied above the Fermi level, even at ambient temperatures. It is non-trivial to extend already existing electronic structure methods to include the effects of temperature, and doing so may increase the cost of the parent method further, making the cost truly prohibitive.

As of now, DFT is the method of choice to model materials, because the low computational cost ($\mathcal{O}(N^3)$, where N is the number of orbitals) allows for calculations of large systems. While DFT has proven successful in a number of applications [1], it has known theoretical issues [2] and can give qualitatively wrong descriptions for some systems [3]. In addition, the exchange-correlation functional is in general unknown and must be approximated in order to carry out realistic calculations. These functionals contain empirical parameters, and there is no universal functional that can be applied to all chemical systems. Wavefunction methods, while highly accurate, are too expensive to apply in the case of realistic solids, and there seems to be no straightforward way to reduce the unfavorable scaling with system size. While there are still unsolved problems in both of these important areas of quantum chemistry, they each have well studied theoretical limitations, making them inapplicable for certain classes of systems. For example, it is known that methods that rely on mean fields or averages, such as Hartree-Fock, will not be able to describe materials with localized electrons and have complex interactions with neighboring electrons. More details about these important methods will be given in later chapters as they will serve as important starting points and benchmarks; However, it is clear that a new class of methods that can treat reasonable system sizes in a theoretically systematic way is needed for solids.

The goal of this thesis is to address these challenges by developing temperature-dependent Greens function based methods for quantum chemistry. Temperature-dependent Green's function methods have favorable properties that have the potential to be able to address some of these issues. One great advantage is the fact that temperature is built in to the theory and does not introduce an

additional cost. Furthermore, they are convenient to use in a formalism called quantum mechanical/quantum mechanical (QM/QM) embedding that allows for treatment of a small portion of the system with a highly accurate method while the remainder of a system can be treated with a lower level, cheaper method. This is a potential route to address the issue of prohibitive computational cost for solids while including the relevant effects of temperature.

While Green's function methods have been used in chemistry in the past, they are much less developed than wavefunction methods and DFT. Typically in chemistry, Green's function methods do not include temperature effects. While temperature-dependent Green's functions and embedding techniques have been used extensively for model systems in physics, they remain relatively unexplored when applied to quantum chemical systems, leaving room for study in this area.

While the ultimate goal is to apply these Green's function methods to solids, they are also applicable to molecules, which will be used as benchmarks in all of the studies in this thesis. To develop new methods in a systematic and reliable manner, one must consider practical as well as theoretical issues. For example, it is necessary to investigate numerical instabilities and convergence of calculated quantities in reference to methods and systems with well-understood behavior. In this work, I will investigate the ability of temperature-dependent Green's function methods to yield accurate chemical quantities such as spectra and thermodynamics. While both of these quantities are accessible from Green's function theory, I will investigate the ability of numerical implementation to yield reliable results. My investigations will be done in comparison with already existing and well understood electronic structure methods such as CC and CI, which will be explained in detail when necessary. In addition, in order to investigate the ability to calculate larger systems with the Green's function, I implement a temperature dependent impurity solver for use in quantum embedding. Embedding allows a high level description of part of the system, while treating the rest of the system with a low level description. Importantly, in quantum embedding, electron interactions between the high and low level can be described in a non-trivial manner. While there are temperature dependent embedding schemes and solvers, it is challenging to use many of these solvers at low temperature.

The rest of the dissertation is as follows. In chapter 2, I highlight important background information regarding quantum chemical calculations that is crucial to understanding the context and details of the remaining chapters. In chapter 3 I investigate the ability of the temperature-dependent Green's function to calculate electronic thermodynamics. Chapter 4 studies the ability of the temperature dependent Green's function to produce accurate spectra. Chapter 5 describes the temperature dependent impurity solver, and in chapter 6 I summarize my findings and form conclusions.

CHAPTER 2

Background

2.1 Overview of Quantum Chemistry

2.1.1 Correlation Energy

One of the simplest and most well-known schemes to describe electrons in an atom or molecule is known as the Hartree-Fock (HF) approximation. In this approximation, one considers each electron moving in an average field of the other electrons. This leads to non-linear equations for the electrons that can be solved in an iterative fashion. Although the Hartree-Fock method was known since the 1930s, it was laborious to apply to even a simple system until the 1950s, when modern computers made this feasible. Once computing power allowed application to larger and larger systems, it became clear that the HF approximation does not adequately describe the electronic motion for even simple chemical applications, which require very accurate description of the electronic interactions to give an accuracy of 1 kcal/mol.

The deficiency of the HF approximation can be described in terms of the *correlation energy*,[1] [4, 5] which is defined as

$$E_{corr} = E_{exact} - E_{HF} \tag{2.1}$$

This quantity describes the difference between the exact electronic energy and the HF energy.

[1] Feynman also called it "stupidity energy".

Where this mean field description fails is well understood. Because electron interactions are not treated explicitly, but rather in an average way, there is an inadequate description of the electron repulsion. As a result, electrons are allowed to occupy orbitals in unfavorable configurations that are too close, resulting in a higher energy than actual. Because more unfavorable configurations are included in the wavefunction, we know that the energy we get from Hartree-Fock is variational, or higher than the true energy, in all cases. In order to lower this energy and hopefully obtain higher accuracy, it is crucial to include at least a portion of this correlation energy.

While correlation energy makes up a small percentage of the total energy, it is naive to exclude this contribution; When considering energy *differences* between electronic states, the difference in correlation energy can contribute significantly to the difference in total energy, making up as much as half of the difference. Some chemistry is attributed solely to correlation energy. For example, NiO is predicted to be a metal by conventional band theory. However, electron correlation effects, which are not accounted for in an accurate enough way in band theory, make NiO an insulator. This trend is seen in other transition metal oxides as well. In many cases, including an adequate description of the correlation is crucial not just for quantitative, but also qualitative accuracy.

It is now one of the grand challenges in theoretical chemistry to develop accurate, cheap methods to describe the correlation energy of various types of systems including atoms, molecules, and solids. Consequently, much work in this field over the past several decades has been toward developing new theories, new approximations, and new implementations to describe the complex many-body interactions that take place within chemical systems.

There have been decades of research trying to develop theories and methods to calculate correlation energy, in 3 main branches, which I will describe below. Starting from Hartree-Fock, many "post Hartree-Fock" methods have been developed and implemented to calculate the missing correlation energy. Post Hartree-Fock methods are quite popular within electronic structure are also known as wavefunction based methods. Examples of such methods include Møller-Plesset perturbation theories (e.g., MP2), coupled-cluster (CC) methods, and configuration interaction (CI) methods. These approximations go beyond the single Slater determinant wavefunction description,

but at a steep computational cost. For example, coupled-cluster singles doubles (CCSD) scales as $O(N^6)$, where N is the number of orbitals. While these methods are often computationally expensive and only applicable to small systems, they are often highly accurate and are excellent to use as benchmark calculations. While the chemical accuracy of Hartree-Fock is inadequate, it is useful from a theory standpoint. Thus, the HF approximation has now become a starting point for many modern wavefunction based quantum chemistry methods and is used as an important reference point to validate new methods against. These wavefunction methods can be systematically improved by adding more and more terms to the wavefunction, leading to a more accurate description.

Alternatively, other very popular electronic structure methods fall under the umbrella of density functional theory (DFT), which takes advantage of the fact that the exact ground state energy of a system is a functional of the electronic density. In practice, the many-body problem is mapped to an auxiliary one particle problem, making it easier to solve. Although this mapping is exact, it is still not possible to find the exact ground state energy or ground state density. The main approximation employed for this method is that of the exchange-correlation functional, which must be parametrized in order to carry out realistic calculations. There are a number of these functionals used in practice, requiring the user to have experience and intuition when choosing a functional to treat a particular chemical system. Aside from practical considerations, DFT is known to have theoretical limitations, namely, that it is only applicable to the ground state and cannot recover the band gap. In spite of these issues, DFT has had wide success in both chemistry and materials science for its range of applicability and relatively cheap computational cost.

A final method that is well-known but less used in electronic structure is the Green's function (sometimes called the electron propagator), which will be the primary method discussed in this work.While the theory of Green's functions in quantum chemistry and condensed matter is well-known and was developed in the 1960's, method development has lagged behind wavefunction and DFT methods. For molecules at zero-temperature, a Green's function calculation can be cumbersome in comparison to wavefunction or DFT methods, as it requires the storage of large matrices

on energy grids to obtain the ground state energy. This is in contrast to wavefunction and DFT methods, which only require the storage of the wavefunction and density, respectively. However, with advances in computing power, the storage requirement is not an enormous barrier. While evaluating the ground state energy may be more cumbersome than other methods, there are many advantages to using these methods and this is a fruitful area of electronic structure still left to be explored.

One benefit of using Green's functions is that they provide a natural language for quantum embedding. This allows one to partition systems and treat the partitions at different levels of theory when required. Quantum embedding using the Green's function will be covered in more detail in chapter 5.

Another attractive feature of Green's functions is the straight-forward temperature dependence of the formalism. Green's function methods are computed on energy grids, which can be made temperature-dependent, without increasing the computational cost compared to the zero-temperature method. Details of the temperature dependent Green's function will be given in Sec. 2.2.1. Including electronic temperature in a calculation is advantageous for many reasons and will be discussed in the next section.

2.1.2 Temperature in electronic structure

Most well-developed methods are done at zero-temperature, which is perfectly valid for ground state properties of materials that have a large fundamental gap or for calculating energy differences. However, to simulate materials with small or no band gap, such as metals and semiconductors, it is crucial to include the effects of electronic temperature. This is because metals and semiconductors can have occupied excited states, even at ambient temperatures. Including such an effect for realistic materials is crucial, but often times the system size and the number of orbitals required to give an accurate description makes such a calculation unfeasible.

It is non-trivial to describe electronic interaction at finite temperatures, because correlation effects are present not only in the ground state, but in the closely lying excited states as well. Al-

though electronic structure methods that include the effects of temperature have been implemented and used for various purposes, they are far less developed than zero-temperature methods. I will highlight a few temperature-dependent methods below.

Finite-temperature implementations of various wavefunction methods have been developed, including finite-temperature Hartree-Fock, finite-temperature coupled cluster, and finite-temperature configuration interaction. These methods are often extensions of the corresponding zero-temperature methods, making them even more expensive. This limits their use to very small system sizes and are thus not capable of simulating realistic materials. However, they are useful for creating highly accurate benchmarks to compare with for the purpose of method development.

The finite-temperature formalism for DFT was developed by Mermin [6] in the same year as the ground state Kohn-Sham formalism in 1965. Although the theory has been worked out for decades, there has been much less development for finite-temperature DFT compared with the ground state formalism. In particular, the number of finite temperature functionals is much less than that of zero-temperature DFT functionals. Parametrizing such functionals is challenging due to the lack of reliable benchmarks to compare with. As a result, finite-temperature DFT has not been applied widely, although such studies exist in areas such as warm dense matter.[7]

Aside from the issue of lack of benchmarks (i.e., lack of reliability of accuracy), the cost of this method can still be prohibitive due to the size of the system under investigation. This is because the inclusion of temperature requires a description that includes more virtual orbitals than would be required of a ground state calculation, as the higher orbitals can become occupied as the temperature increases. However, because this is such a new area, it is still unclear how many additional orbitals must be included to account for temperature effects. Methods to combat this, such as orbital free DFT [8] are being developed to reduce this cost, but this area requires further exploration.

To address the challenges in this area, it would be helpful to have ab-initio temperature dependent methods for realistic systems to serve as benchmarks.

2.2 Green's Function from Perturbation Theory

Here, I will highlight parts of the Green's function formalism that are relevant to this work. There are many excellent textbooks that outline this formalism in detail such as [9, 10, 11, 12, 13].

The Green's function is more general than the wavefunction because it has information about the history of the particle. Actually, one-particle Green's functions are a type of propagator. The name propagator is derived from the fact that we are propagating a particle from an intial position x_0 and time t_0 to a later position x and time t. While the Green's function also has information about the many-body interactions, it is just as challenging to calculate the Green's function as it is to calculate the wavefunction, requiring approximations in the practical calculation of Green's functions. A common approach is to begin from a non-interacting Green's function G_0 and use perturbation theory to calculate the full Green's function G. The following arguments are general, but will be applied to the case of interacting fermions in this work.

The Green's function for an interacting system can be described by a Hamiltonian partitioned into a solvable part and a perturbative part. A convenient choice is to take the solvable part to be a free propagator and the perturbation as a scattering event. The Hamiltonian can be partitioned as

$$H = H_0 + V \tag{2.2}$$

where H_0 is the Hamiltonian of the free particle, and V is an interaction (scattering event). Thus we can construct the full propagator G as a sum of the non-interacting propagator G_0, the propagator with one scattering event, the propagator with two scattering events, etc.

$$\begin{aligned} G &= G_0 + G_0VG_0 + G_0VG_0VG_0 + \cdots \\ &= G_0(1 + VG_0 + VG_0VG_0 + \cdots) \end{aligned} \tag{2.3}$$

This expression is just a geometric series, and can be written as a sum as

$$G = \frac{G_0}{1 - VG_0} = \frac{1}{G_0^{-1} - V} \tag{2.4}$$

This is known as the Dyson equation. To use perturbation theory to describe an interacting system, we treat the interacting Green's function as though it has had a series of encounters with an interaction which we call the self-energy Σ. What this means physically is that the particle interacts with other particles in the system and creates a cloud, and this cloud in turn interacts with the particle, as if the particle is interacting with itself. The self-energy describes all of the many-body interactions of the system and is related to the Green's function through the Dyson equation (Eqn. 2.4), given as

$$\Sigma = G_0^{-1} - G^{-1} \tag{2.5}$$

This description of the Green's function is general and can be implemented in many formalisms, including temperature-dependent and temperature-independent. In addition, the Green's function can be described in terms of position and time, as well as momentum and time or position and energy. In the context of perturbation theory, the momentum and energy domain is often convenient.

2.2.1 Temperature-Dependent Matsubara Green's Function

The temperature-dependent Green's function formalism was introduced by Matsubara in 1955, and is sometimes called the Matsubara formalism. [14] This formalism includes temperature in the Green's function, and also turns out to be mathematically tractable and just as convenient to work with as the zero-temperature Green's function.

Green's function theory is a statistical theory which gives access to ensemble quantities. Statistical ensemble quantities rely on Boltzmann factors $e^{-\beta H}$ to compute partition functions and

physical quantites derived from them. The Matsubara Green's function for an electron can be expressed as

$$G = \frac{Tr[e^{-\beta H} C_{p\sigma}(t_0) C^{\dagger}_{p\sigma}(t)]}{Tr(e^{-\beta H})} \tag{2.6}$$

where the creation and annihilation $C^{(\dagger)}_{p\sigma}$ in momentum p and spin σ are in the Heisenberg picture, with time dependence on the operators as

$$C_{p\sigma}(t) = e^{itH} C_{p\sigma} e^{-itH} \tag{2.7}$$

In this expression for G, the Hamiltonian appears in both exponential factors, and it would be quite cumbersome to carry out two different perturbation expansions. The Green's function relies on Boltzmann factors, which are very similar in structure to the time evolution operator e^{-itH} because both of them have exponential form. These similarities can be taken advantage of by treating time as a complex temperature. That is, we replace it with $\beta = \frac{1}{k_b T}$. The convenience lies in the ability to treat ensemble Green's functions using time-dependent techniques while obtaining statistical ensemble quantities.

To obtain G in terms of the energy or frequency parameter $i\omega$, we take have the Fourier transform to obtain

$$G = \frac{1}{i\omega - H} \tag{2.8}$$

In practice, one must compute frequency sums over unperturbed Green's functions to evaluate G. For the Matsubara Green's function for electrons (fermions), this is done using the so called Matsubara frequencies given as

$$i\omega = \frac{(2n+1)i\pi}{\beta}, n = 0, 1, 2, ... \tag{2.9}$$

What quantities can we obtain from this temperature-dependent Matsubara Green's function? In theory, since the it is possible to get the partition function (Z) from the Green's function, one is

able to obtain any quantity that is available from Z, including thermodynamic quantities such as entropy and Helmholtz energy. This will allow us to compare stabilities between different phases. The partition function is expressed as $Z = e^{-\beta\Omega}$, where Ω is the grand potential. The grand potential can be evaluated from the Green's function as

$$\Omega = \frac{1}{\beta}\{\Phi - \mathrm{Tr}[\Sigma G + \ln(\Sigma - G_0^{-1})]\} \tag{2.10}$$

The Luttinger-Ward functional Φ is evaluated as

$$\Phi = \sum_{m=1}^{\infty} = \frac{1}{2m}\mathrm{Tr}\left[\Sigma^{(m)}G\right] \tag{2.11}$$

where m is an integer referring to the level of truncatation of the self-energy to order m. The Green's function has a clear connection with spectra when evaluated on the real frequency axis, where the poles correspond to electron removal and addition energies. The spectra can be evaluated as

$$A(\omega) = \frac{-1}{\pi}\mathrm{Tr}[\mathrm{Im}\ \mathbf{G}(\omega)] \tag{2.12}$$

Details regarding practical calculations of thermodynamics and spectra from the Matsubara Green's function will be explored in chapters 3 and 4, respectively.

The Matsubara Green's function is well-known in physics and has been applied to model systems, such as the Hubbard model, in the past. [15, 16, 17] However, much less work has been done in the area of applying this Matsubara formalism to a realistic quantum chemical Hamiltonians containing two-electron interactions. Such studies exist, but were limited to a few small atoms and molecules with simple bases. [18, 19, 20] Thus, while it is in theory possible to obtain quantities such as spectra and thermodynamics from the Matsubara Green's function, this has never been rigourously investigated for realistic chemical systems.

CHAPTER 3

Electronic Thermodynamics

3.1 Temperature-Dependent Thermodynamics from the Matsubara Green's function

3.1.1 Introduction

In molecular quantum-chemical calculations of thermodymanic properties such as Gibbs energy [21, 22], the temperature dependent component is usually dominated by vibrational contributions. This is due to the large gaps between electronic states, which ensure that the excited state populations will be negligible. Consequently, common molecular calculations do not explicitly include temperature effects on the electronic structure.

However, for materials such as doped semiconductors [23] the magnitude of the electronic band gap can be relatively small, or for metals nonexistent altogether, allowing electronic states other than the ground state to be accessible at low temperatures. Thus, it is necessary to include temperature effects into the electronic description. Even though for most materials the vibrational contribution to the specific heat is much larger than the electronic one, there are cases when the incorporation of the electronic contribution is necessary. The electronic contribution to specific heat is important for **(i)** heavy fermion materials at low temperatures [24], **(ii)** materials that do not undergo a structural transition that changes the vibrational contribution, causing the stability of phases to primarily depend on the relative electronic contribution to Gibbs energy, **(iii)** materials

with a structural transition where the difference between vibrational contributions of the phases is of the same order as the difference between electronic contributions [25, 26]. Thus, modern materials calculations can benefit from computational tools that provide access to the temperature dependent electronic contribution to the specific heat, Gibbs energy, entropy, or electronic part of the partition function.

While in traditional quantum chemical calculations evaluating the electronic contribution to temperature dependent quantities is certainly not wide spread, a number of such methods exist, most notably, the finite temperature Hartree-Fock (HF) [27], density functional theory (DFT) [6, 7, 28, 29], Møller-Plesset second order perturbation theory (MP2) [30], coupled-cluster (CC) [31, 32, 33], and Lanczos method [34, 35] for finite temperature configuration interaction (CI) calculations. However, these methods are usually quite difficult to implement and costly to use since they rely on the modification of the parent zero-temperature method to the finite temperature formalism by adapting it to work in the canonical or grand canonical ensemble. For example, to carry out such calculations in the CI formalism, one must obtain the excited states and corresponding Boltzmann factors in order to evaluate the partition function and thermodynamic averages, making application of finite temperature variants of these methods quite cumbersome.

Conversely, for the Green's function formalism the connection to thermodynamics arises in a straightforward manner and was derived in numerous books in the past [9, 10, 11, 36]. While this theoretical connection is well understood, the actual numerical calculations of the thermodynamic quantities still remain quite challenging since a fully self-consistent imaginary axis (Matsubara) Green's function calculation is desired. A non-self-consistent Green's function can result in non-unique thermodynamic quantities.

The fully self-consistent Green's function calculations are challenging for multiple reasons, such as large imaginary time and frequency grids required for convergence or multiple solutions that can be present due to the non-linear nature of the equations. It is for reasons such as these that in recent years calculations that capitalized on Green's function language and yield thermodynamic quantities where mostly done for model systems [37, 38, 39, 40, 41].

Here, we would like to stress that while multiple large scale real axis Green's function calculations are performed at present for the single shot G_0W_0, GW_0, or semi-self consistent GW for large realistic systems [42, 43, 44, 45, 46, 47, 48], currently, only a few research groups have managed to rigorously generalize the self-consistent finite temperature (imaginary axis) Green's function formalism to deal with a general Hamiltonian containing all the realistic interactions [49, 19, 50, 51, 52, 53]. Thus, any insight gained from studying even simple periodic systems and analyzing the possible self-consistent solutions of the Matsubara formalism remains valuable.

To the best of our knowledge, here, we present the first application of the fully self-consistent finite temperature Green's function formalism to evaluate thermodynamic quantities and phase stability for a periodic system described by a full quantum chemical Hamiltonian. We demonstrate that Green's function formalism leads to a simple calculation of the electronic contribution to the Helmholtz or Gibbs energy, entropy, grand potential, and partition function without explicitly performing any excited state calculations. The presented formalism is exact at the infinite temperature limit since the perturbative Green's function formulation is a perturbation that contains the inverse temperature as small parameter.

This chapter is organized as follows. In Sec. 3.1.2, we introduce the imaginary Green's function formalism and its connection to thermodynamics. In Sec. 3.2 and 3.2.1, we list properties of the Luttinger-Ward functional which is our main computational object and we explain its evaluation within a self-consistent Green's function second-order (GF2) periodic implementation. In Sec. 3.2.2, we present numerical results first for a benchmark molecular problem and then for two 1D systems: periodic hydrogen as well as boron nitride. Finally, we form conclusions in Sec. 3.2.3.

3.1.2 Connection with thermodynamics

One of the first descriptions of the connection between the Green's function formalism and thermodynamics was presented in the book by Abrikosov, Gorkov, and Dzyaloshinski [36]. Since then multiple texts have appeared that discuss this connection [9, 11, 54]. For an excellent, detailed derivation, we encourage the reader to follow Ref. [9]; here, we will only mention few basic

Green's function equations for the sake of completeness.

The one-body Green's function is defined as

$$G_{ji}(z_1, z_2) \equiv \frac{\mathrm{Tr}[e^{-\beta\hat{H}^M}\hat{G}_{ji}(z_1,z_2)]}{\mathrm{Tr}[e^{-\beta\hat{H}^M}]} = \frac{1}{i}\frac{\mathrm{Tr}[\tau\{e^{-i\int_\gamma d\bar{z}\hat{H}(\bar{z})}\hat{d}_{j,H}(z_1)\hat{d}^\dagger_{i,H}(z_2)\}]}{\mathrm{Tr}[\tau\{e^{-i\int_\gamma d\bar{z}\hat{H}(\bar{z})}\}]}, \tag{3.1}$$

where $\hat{d}_{j,H}(z_1)$ and $\hat{d}^\dagger_{i,H}(z_2)$ are the second-quantized annihilation and creation operators in the Heisenberg representations and $\beta = 1/(k_B T)$ is the inverse temperature while T is the actual temperature and k_B is the Boltzmann constant. This Green's function, depending on how the contour γ in the complex plane is closed, can be used to describe system's time evolution (when z_1 and z_2 are set to the real-time variables), zero temperature phenomena, or equilibrium phenomena at finite temperature.

Here, we are interested in a formalism used to calculate the initial ensemble average that is applied to systems in thermodynamic equilibrium at finite temperature. This approach is called Matsubara formalism or the "finite-temperature formalism". For this reason, in the Green's function from Eq. 3.1 we set $z_1 = t_0 - i\tau_1$ and $z_2 = t_0 - i\tau_2$. Consequently, the Green's function

$$G^M_{ji}(\tau_1, \tau_2\ \ ) = \frac{1}{i}\{\theta(\tau_1 - \tau_2)\frac{\mathrm{Tr}[e^{(\tau_1-\tau_2-\beta)\hat{H}^M}\hat{d}_j e^{(\tau_2-\tau_1)\hat{H}^M}\hat{d}^\dagger_i]}{\mathrm{Tr}[e^{-\beta\hat{H}^M}]} \pm\theta(\tau_2 - \tau_1)\frac{\mathrm{Tr}[e^{(\tau_2-\tau_1-\beta)\hat{H}^M}\hat{d}^\dagger_i e^{(\tau_1-\tau_2)\hat{H}^M}\hat{d}_j]}{\mathrm{Tr}[e^{-\beta\hat{H}^M}]}\} \tag{3.2}$$

does not describe any time evolution of the system under study. Instead, in this Green's function the initial state of the system can be the thermodynamic state corresponding to a Hamiltonian, $\hat{H}^M = \hat{H}(t_0) - \mu\hat{N}$, where $\hat{N}$ is the particle number operator. Thus, from this Matsubara Green's function, the initial ensemble average of any one-body operator $\hat{O} = \sum_{ij} O_{ij}\hat{d}^\dagger_i\hat{d}_j$, can be evaluated simply as

$$O = \frac{\mathrm{Tr}[e^{-\beta\hat{H}^M}\hat{O}]}{\mathrm{Tr}[e^{-\beta\hat{H}^M}]} = \pm i\sum_{ij} O_{ij}G^M_{ji}(\tau), \tag{3.3}$$

where $\tau = \tau_1 - \tau_2$ since the one-body Green's function matrix elements depend only on the difference of the imaginary time variables. Furthermore, the imaginary time Green's function $G(\tau)$ can be Fourier transformed to the imaginary frequency Green's function $G(i\omega_n)$ where for fermions the frequency grid is given by $\omega_n = \frac{(2n+1)\pi}{\beta}$ with n defined here as a positive integer. For simplicity, in the remainder of this paper, we will drop subscript M denoting Matsubara Green's functions since from now on we will only discuss this finite temperature formalism.

The discussion above shows that at finite temperature one can get grand canonical ensemble averages of one-body operators using the Matsubara formalism. However, let us ask one more question: Can we get a system's static thermodynamic variables such as electronic Gibbs or Helmholtz energy, internal energy, and electronic entropy from dynamic (frequency dependent) variables such as Green's function and self-energy?

The thermodynamics of a system can be described by a thermodynamical potential, such as the grand potential Ω [9]

$$\Omega = \frac{1}{\beta}\{\Phi - \mathrm{Tr}[\Sigma G + \ln(\Sigma - G_0^{-1})]\}, \tag{3.4}$$

where the self-energy $\Sigma = \Sigma(i\omega_n)$ describes all the frequency dependent correlational effects present in the system and $G_0 = G_0(i\omega_n)$ is the reference (usually non-interacting) system's Green's function and $G = G(i\omega_n)$ is the interacting Green's function. The interacting and non-interacting Green's functions are connected through the Dyson equation, $\Sigma = G_0^{-1} - G^{-1}$. The Φ functional from Eq. 3.4 is called the Luttinger-Ward functional[55] [56] and is defined as

$$\Phi = \sum_{m=1}^{\infty} \frac{1}{2m} \mathrm{Tr}[\sum_n \Sigma^{(m)}(i\omega_n) G(i\omega_n)], \tag{3.5}$$

where $\Sigma^{(m)}(i\omega_n)$ is a self-energy containing all irreducible and topologically inequivalent diagrams of order m. The detailed derivation of Eq. 3.4 is presented in Ref. vanleeuwentext.

Thus, the computational object that provides a connection between the static and dynamic quantities is the Luttinger-Ward functional. This scalar functional $\Phi = \hat{\Phi}[G]$ depends on the Green's function and has multiple important properties for Green's function theory.

3.2 Properties of the Luttinger-Ward Functional

The formal properties of Luttinger-Ward functional have been discussed extensively before. The functional has previously been applied to calculate energies for atoms and molecules [49, 19], the electron gas [57], as well as for the Hubbard lattice [39, 58, 59, 38]. In the following section, we will only outline some of the most salient properties of the Luttinger-Ward functional to benefit the reader.

3.2.0.1 Self-energy as a functional derivative

The self-energy $\Sigma = \Sigma(i\omega_n)$ can be obtained as a functional derivative of the Luttinger-Ward functional

$$\beta \frac{\delta \hat{\Phi}[G]}{\delta G} = \hat{\Sigma}[G]. \tag{3.6}$$

Here, the self-energy is defined as a functional of Green's function that is evaluated independent of the Dyson equation. Consequently, in the non-interacting limit, where $\Sigma = 0$, it follows that the Luttinger-Ward functional is zero itself, $\hat{\Phi}[G] = 0$.

3.2.0.2 Connection with the grand potential Ω

The grand potential is a number but the mathematical object defined in Eq. 3.4 can be viewed more generally as a functional of Green's functions $\Omega[G]$. When a Green's function is a self-consistent solution of the Dyson equation then the functional derivative $\frac{\delta\Omega[G]}{\delta G} = 0$ since $\delta\Phi = \mathrm{Tr}[\Sigma\delta G]$ and $\delta\Omega[G] = \frac{1}{\beta}\{\delta\Phi - \mathrm{Tr}[\delta\Sigma G + \Sigma\delta G - G\delta\Sigma]\}$. Consequently, we can conclude that the functional $\Omega[G]$ at the stationary point is equal to the grand potential. Having grand potential one gains access to the partition function (Z) since

$$\Omega = -\frac{1}{\beta}\ln Z. \tag{3.7}$$

The Helmholtz energy, $A = E - TS$, where E is the internal energy and S is the entropy of a system at a given temperature T, is connected to the grand potential as $A = \Omega + \mu N$, where N is

the number of electrons in the system. Thus, knowing the grand potential, we can easily calculate the electronic entropy as

$$S = \frac{E - \Omega - \mu N}{T} \tag{3.8}$$

as long as we have access to the internal energy of a system. The internal energy at a given temperature T can be evaluated using the Galitskii-Migdal formula

$$E = \frac{1}{2}\mathrm{Tr}\left[(h + F)\,\gamma\right] + \frac{2}{\beta}\sum_{n}^{N_\omega} \mathrm{Re}(\mathrm{Tr}[G(i\omega_n)\Sigma(i\omega_n)]), \tag{3.9}$$

where γ is the one-body density matrix, h is the one-body Hamiltonian, F is the Fock matrix of a system, and N_ω is the size of the imaginary grid. Consequently, having access to the Luttinger-Ward functional of a system yields multiple electronic thermodynamic quantities.

3.2.0.3 Universality

Given two systems A and B at the same physical temperature T and the same chemical potential μ described by two Hamiltonians $\hat{H}_A = \sum_{ij} t^A_{ij} a^\dagger_i a_j + \sum_{ijkl} v_{ijkl} a^\dagger_i a^\dagger_j a_l a_k$ and $\hat{H}_B = \sum_{ij} t^B_{ij} a^\dagger_i a_j + \sum_{ijkl} v_{ijkl} a^\dagger_i a^\dagger_j a_l a_k$ such that they have the same two-body integrals v_{ijkl} but different one-body integrals $t^A \neq t^b$ the Luttinger-Ward functional is same (universal) for both of them. Since $\hat{\Phi}^A = \hat{\Phi}^B$, then it must also hold that $\hat{\Sigma}^A(G) = \hat{\Sigma}^B(G)$. In other words, two systems described by different G_0 but having the same two-body interactions are described by the same Luttinger-Ward functional.

3.2.1 Evaluation of Luttinger-Ward Functional Within GF2

3.2.1.1 Description of the GF2 algorithm

The self-energy, which we evaluate self-consistently in this work, is computed perturbatively at the second-order (GF2) level. GF2 is advantageous for many reasons, namely, among others it behaves qualitatively correct for moderately strongly correlated systems [50], unlike methods such as MP2 or CCSD which tend to diverge in these cases. GF2 has small fractional charge and fractional

spin errors [60]. GF2 is carried out self-consistently on imaginary time τ and imaginary frequency $i\omega_n$ axes with a computational scaling of $O(n_\tau N^5)$ for molecular cases, where n_τ is a prefactor that depends on the size of the imaginary time grid and N is the number of orbitals present in the problem. We build the Green's function using the following expression

$$G(i\omega_n) = [(i\omega_n + \mu)S - F - \Sigma(i\omega_n)]^{-1} \tag{3.10}$$

where F and S are the Fock and overlap matrices in the atomic orbital (AO) basis, respectively, and μ is the chemical potential, which guarantees a correct particle number. To obtain $\Sigma(i\omega_n)$, we solve the Dyson equation given as

$$\Sigma(i\omega_n) = G_0(i\omega_n)^{-1} - G(i\omega_n)^{-1} \tag{3.11}$$

where $G_0(i\omega_n) = [(i\omega_n + \mu)S - F]^{-1}$ is the non-interacting Green's function while $G(i\omega_n)$ is the interacting Green's function since it contains the self-energy. To reduce the number of necessary grid points, we employ a spline interpolation method to evaluate the Green's function [52] and Legendre orthogonal polynomials to expand the $\Sigma(\tau)$ matrix [61]. As pointed out previously, this self-consistent evaluation guarantees that both the Galitskii-Migdal and Luttinger-Ward energies are stationary with respect to the Green's function. For a full discussion of the algorithm and implementation details of GF2, we refer the reader to Refs. GF2,fractional. The main computational object in our evaluation is the self-energy in the AO basis, which can be expressed as

$$\begin{aligned}\Sigma_{ij}(\tau) = -\sum_{klmnpq} & G_{kl}(\tau)G_{mn}(\tau)G_{pq}(\tau)\times \\ & \times v_{ikmq}(2v_{ljpn} - v_{pjln}).\end{aligned} \tag{3.12}$$

where v_{ijkl} are the two-electron integrals in the AO basis in the chemist's notation. Eq. 3.12 is evaluated in a Legendre polynomial basis [61] to accelerate the calculation.

The details of a periodic GF2 implementation have been reported in Ref. [51]. The basic

differences from the molecular version include solving the Dyson equation in **k**-space via

$$G^k(i\omega_n) = \left[(i\omega_n + \mu)S^k - F^k - \Sigma^k(i\omega_n)\right]^{-1} \tag{3.13}$$

and complicating the real-space self-energy, $\Sigma^{\mathbf{0g}}(\tau)$, evaluation by additional cell index summations:

$$\begin{aligned}\Sigma^{\mathbf{0g}}_{ij}(\tau) = -\sum_{\mathbf{g_1},\ldots,\mathbf{g_6}} \sum_{klmnpq} G^{\mathbf{g_3 g_6}}_{k\ l}(\tau) G^{\mathbf{g_1 g_4}}_{m\ n}(\tau) G^{\mathbf{g_5 g_2}}_{p\ q}(-\tau) \times \\ \times v^{\mathbf{0 g_1 g_2 g_3}}_{i\ m\ q\ k} (2v^{\mathbf{g g_4 g_5 g_6}}_{j\ n\ p\ l} - v^{\mathbf{g g_6 g_5 g_4}}_{j\ l\ p\ n}).\end{aligned} \tag{3.14}$$

$\Sigma^k(i\omega_n)$ in Eq. 3.13 and $\Sigma^{\mathbf{0g}}(\tau)$ in Eq. 3.14 are interconvertible via corresponding Fourier transforms from the **k**- to real-space and between the imaginary time and imaginary frequency domains also via Fourier transform. The self-energy calculation according to Eq. 3.14 results in $O(N^5 N_{cell}^4 n_\tau)$ formal scaling of the computation cost with N the number of orbitals in the unit cell and N_{cell} the number of real space cells. This is typically a computational bottleneck of the GF2 self-consistency procedure.

The level of self-consistency at which the correlated Green's function equation should be iterated can depend on particular phases present in the phase diagram, such as Mott (see Ref. [62]). In particular, the non-interacting Green's function $G_0(i\omega_n)$ build using updated Fock matrix or the correlated Green's function $G(i\omega_n)$ can re-enter the evaluation of the self-energy. We observe that the use of $G_0(i\omega_n)$ with the updated Fock matrix in the self-consistent evaluation of the self-energy is a well-behaved procedure when the strong correlations and the Mott phases emerge. The full self-consistent cycle, with $G(i\omega_n)$ re-entering the evaluation of the self-energy becomes ill behaved for these cases and we experienced difficulty converging it. We therefore use the former "partial" self-consistency ($G_0(i\omega_n)$ with the updated Fock matrix in the self-consistent evaluation of the self-energy) for the Mott regime. Such scheme is not uncommon in DMFT type calculations [62].

The expression for the total energy likewise acquires a cell summation according to Eqs. 13

and 14 in Ref. [51]:

$$
\begin{aligned}
E_{tot} &= E_{1b} + E_{2b} \\
&= \tfrac{1}{2} \textstyle\sum_{\mathbf{g},i,j} \gamma_{ij}^{\mathbf{0g}} (2h_{ij}^{\mathbf{0g}} + [\Sigma_\infty]_{ij}^{\mathbf{0g}}) + \\
&+ \tfrac{2}{\beta} \textstyle\sum_{\mathbf{g},i,j} \mathrm{Re}\left[\sum_n G_{ij}^{\mathbf{0g}}(i\omega_n) \Sigma_{ij}^{\mathbf{0g}}(i\omega_n) \right].
\end{aligned}
\tag{3.15}
$$

3.2.1.2 Evaluation of the grand potential in the k-space

The evaluation of the Luttinger-Ward functional in conserving approximations [63] such as the self-consistent second-order Green's function (GF2)[50, 60, 61] is quite straightforward and was originally derived by Luttinger and Ward [55] as

$$
\Phi^{(2)} = \frac{1}{4} \mathrm{Tr}[\sum_n \Sigma^{(2)}(i\omega_n) G(i\omega_n)], \tag{3.16}
$$

where $\Sigma^{(2)}(i\omega_n)$ is the frequency dependent part of the second-order self-energy. Since both $G(i\omega_n)$ and $\Sigma^{(2)}(i\omega_n)$ are readily available from a GF2 calculation, we are able to easily evaluate all terms of the functional.

The expression for grand potential from Eq. 3.4 can be conveniently reformulated as

$$
\begin{aligned}
\Omega_{LW} &= \frac{1}{2} \mathrm{Tr}[\gamma \Sigma_\infty] + \mathrm{Tr}[G\Sigma] \\
&+ \mathrm{Tr}[\ln\{1 - G\Sigma\}] + \mathrm{Tr}[\ln\{G_0^{-1}\}].
\end{aligned}
\tag{3.17}
$$

An excellent derivation of the above equation is given in Ref. [19] for molecular systems. However, as we mentioned before, for molecular systems the changes due to the electronic contributions of the Gibbs or Helmholtz energy are negligible due to the size of the gap.

Here, we list detailed steps that need to be executed when dealing with crystalline systems where the electronic effects influencing Helmholtz energy can be significant. In the periodic implementation, we evaluate the grand potential per unit cell, $\Omega^{\mathbf{00}}$. The overall expression is given as

a sum of all the components

$$\begin{aligned}\Omega^{\mathbf{00}} = \Omega^{\mathbf{00}}_{\mathrm{Tr[G\Sigma]}} + \Omega^{\mathbf{00}}_{\mathrm{Tr[ln\{1-G\Sigma\}]}} \\ +\Omega^{\mathbf{00}}_{\mathrm{Tr[ln\{G_0^{-1}\}]}} + \Omega^{\mathbf{00}}_{\frac{1}{2}\mathrm{Tr}[\gamma\Sigma_\infty]}\end{aligned} \tag{3.18}$$

where we sum the contribution per unit cell for each term present in Eq. 3.17. Due to the crystalline symmetry, it is often more convenient to calculate these quantities in **k**-space and transform the resulting quantity to the real space rather than using an explicit real space representation of all the quantities involved. All terms in Eq. 3.18 containing the Green's function G, or self-energy Σ were computed in **k**-space and then Fourier transformed to real space. For example, to calculate the $\Omega^{\mathbf{00}}_{\mathrm{Tr[G\Sigma]}}$ contribution, we can first evaluate the **k**-dependent quantity

$$\Omega^{k}_{\mathrm{Tr[G\Sigma]}} = \frac{2}{\beta}\sum_{i,j,n}^{N_\omega} G^k(i\omega_n)_{ij}\Sigma^k(i\omega_n)_{ji} \tag{3.19}$$

where the indices i and j run over all atomic orbitals in a given $k-$block. Subsequently, we perform Fourier transform of $\Omega^{k}_{\mathrm{Tr[G\Sigma]}}$ to yield the real space $\Omega^{\mathbf{00}}_{\mathrm{Tr[G\Sigma]}}$ contribution.

The most cumbersome evaluation is of the term $\Omega^{\mathbf{00}}_{\mathrm{Tr[ln\{1-G\Sigma\}]}}$, which requires diagonalization of the matrix $G^k\Sigma^k + (G^k\Sigma^k)^\dagger - G^k\Sigma^k(G^k\Sigma^k)^\dagger$, where the matrices G^k and Σ^k are understood to be dependent on $i\omega_n$. Once the eigenvalues of this matrix, ϵ_i^k, have been computed for each imaginary frequency point, $i\omega_n$, we have

$$\Omega^{k}_{\mathrm{Tr[ln\{1-G\Sigma\}]}} = \frac{2}{\beta}\sum_{n,i}^{N_\omega} \ln\{1-\epsilon_{\mathrm{i}}^{\mathrm{k}}\}, \tag{3.20}$$

which can be Fourier transformed to the real space.

To include the contribution from the Fock matrix, $\Omega^{\mathbf{00}}_{\mathrm{Tr[ln\{G_0^{-1}\}]}}$, we calculate

$$\Omega^{k}_{\mathrm{Tr[ln\{G_0^{-1}\}]}} = \begin{cases} \frac{1}{\beta}\ \sum_i \ln(1+\mathrm{e}^{\beta(\epsilon_{\mathrm{i}}^{\mathrm{k}}-\mu)}) + \epsilon_{\mathrm{i}}^{\mathrm{k}}, & \text{if } \epsilon_i^k - \mu < 0 \\ \frac{1}{\beta}\ \sum_i \ln(1+\mathrm{e}^{-\beta(\epsilon_{\mathrm{i}}^{\mathrm{k}}-\mu)}), & \text{otherwise.} \end{cases} \tag{3.21}$$

where by analyzing if the term $\epsilon_i^k - \mu$ is smaller or greater than zero we account for the cases where the absolute value of the Fock matrix eigenvalue can be large leading to numerical problems if only one branch of the above expression is used. This term accounts for occupation changes with temperature. For high β values (low values of the actual temperature T), the expression reduces to

$$\Omega^k_{\mathrm{Tr}[\ln\{G_0^{-1}\}]} = \sum_{N_{occ}} \epsilon_i^k, \tag{3.22}$$

which allows electrons to occupy only the lowest available state, as is expected at a very low temperature.

We calculate the term $\Omega^{\mathbf{00}}_{\frac{1}{2}\mathrm{Tr}[\gamma\Sigma_\infty]}$ directly in the real space as $\frac{1}{2}\mathrm{Tr}[\gamma\Sigma_\infty]$, since in the AO basis, the decay of both γ which is the density matrix and Σ_∞ which is the frequency independent part of the self-energy is rapid enough for a relatively few number of cells to assure a converged value of $\Omega^{\mathbf{00}}_{\frac{1}{2}\mathrm{Tr}[\gamma\Sigma_\infty]}$.

3.2.2 Results

3.2.2.1 HF molecule

In this subsection, for a simple molecular example, a hydrogen fluoride molecule, we provide a calibration of the thermodynamic quantities such as internal energy E, Helmholtz energy A, and entropy S, which are evaluated at the GF2 level and compared to the full configuration interaction (FCI) calculation. The evaluation of the thermodynamic quantities at the FCI level can be done only for very small molecular examples, such as HF, since such a system has only 10 electrons and 6 basis functions in the STO-3G basis, resulting in a small number of possible configurations necessary to evaluate the FCI grand potential. Note that to describe a true physical system at very high temperature we would require a very large basis set. Here, we use HF as a model molecular system that is calculated in a minimal basis set solely to enable comparison of GF2 with FCI. The full configuration interaction (FCI) quantities for HF molecule were calculated previously by Kou and Hirata [64]. In addition, we show the same system calculated with finite-temperature at

the Hartree-Fock level. We would like to emphasize that we provide this molecular example as a benchmark only, in order to compare our method with highly accurate FCI quantum chemical data. Typically electronic contributions to thermodynamics are not considered for molecular systems.

Let us first note that in order to calculate the FCI partition function and subsequently grand potential in the grand canonical ensemble, we need to evaluate

$$Z^{GC} = \sum_{N=0}^{2n} \sum_{S_z} \sum_{i} \langle \Phi_i^{(N,S_z)} | exp\{-\beta(\hat{H} - \mu\hat{N})\} | \Phi_i^{(N,S_z)} \rangle, \tag{3.23}$$

where the $\Phi_i^{(N,S_z)}$ is the FCI wave function with N electrons and S_z quantum number and the number of possible occupation runs from 0 to $2n$, where n is the number of orbitals. Consequently, we need to explicitly obtain the information about every possible excited state present in the system with different number of electrons. Such a task quickly becomes impossible for any larger systems. In contrast, in Green's function methods, we never need to explicitly evaluate any information concerning specific excited states. It is sufficient to evaluate Eq. 3.17 and then Eq. 3.7 to obtain the grand canonical partition function. Thus, even for relatively large systems such calculations remain feasible.

Results from our calibration are shown in Fig. 3.1. The numerical values used in the plots are tabularized in the Supplemental Information. The detailed description of the grids on which we evaluate $\Sigma(\tau)$ and $G(i\omega_n)$ can be found in Ref. [65]. For the hydrogen fluoride molecule the temperature range is huge due to the size of the Hartree-Fock HOMO-LUMO gap in this system, which is around 1.0 a.u. corresponding to a temperature of around 3.0×10^5 K. Conseqhuently, to make every state accessible to the electrons in this system, we require extremely high temperatures, as indicated by our results.

In the very high temperature limit, both finite temperature Hartee-Fock and GF2 yield the internal energy (E), Helmholtz energy (A), and entropy (S) in excellent agreement with FCI results. This is of course expected since at very high temperatures the electronic behavior is well described by mean field theories. For the intermediate temperatures, GF2 thermodynamic quantities (E, S,

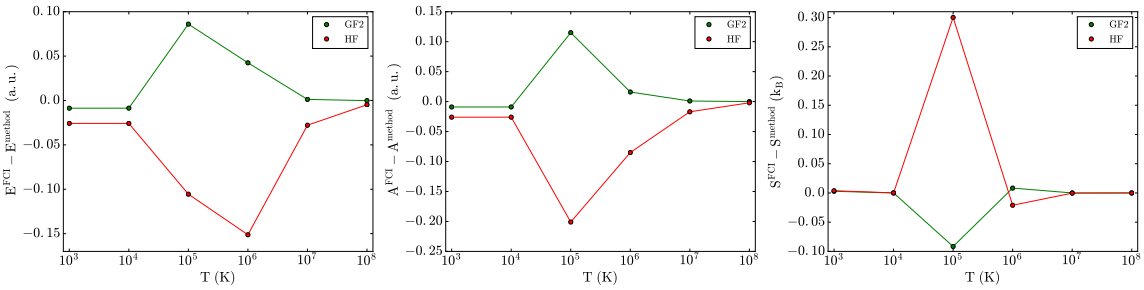

Figure 3.1: The differences between GF2, finite temperature Hartree-Fock and FCI for the hydrogen fluoride molecule at various temperatures.

and A) are closer to FCI than thermodynamic quantities obtained in finite temperature Hartee-Fock. For this system at intermediate temperatures, the GF2 thermodynamic quantities are always overestimated while the finite temperature Hartree-Fock always underestimate them in comparison to FCI. The GF2 and Hartree-Fock entropies for low temperatures are well recovered and comparable. As expected, the low temperature GF2 internal energy is closer to FCI than the one evaluated using finite temperature Hartree-Fock. For our very lowest temperature (10^3 K), we recover a small negative entropy. This is a numerical artifact brought about from the level of convergence of the internal energies (1.0×10^{-5} a.u.) and the expression for entropy which requires multiplication by β, $S = \beta(E - \Omega - \mu N)$. Thus, the smallest error $\approx 10^{-5}$ in the energy will result in $\approx 10^{-3}$ error in the entropy due to multiplication by $\beta = 100$.

3.2.2.2 Periodic calculation of 1D hydrogen

In our previous work, GF2 was implemented for periodic systems and applied to a 1D hydrogen solid [51] in the mini-Huzinaga [66] basis set. We consider the same system in this work, where we have used 5,000 Matsubara frequencies to discretize the Green's function in the frequency domain, 353 imaginary-time points, and 27 Legendre polynomials. We have found this grid size is sufficient to evaluate energy differences between the systems at various temperatures. Up to 73 real space unit cells appear in the self-energy evaluation (Eq. 3.14).

This system is simple enough to be a test bed for self-consistent Green's function theory; however, it displays a phase diagram that is characteristic of realistic solids. At different internuclear

separations, corresponding to different pressures, we were able to recover multiple solutions. Although yielding different electronic energies and different spectra, these solutions can be mathematical artifacts of the nonlinear self-consistency procedure present in GF2; however, they can also have physical meaning corresponding to different solid phases.

To decide which phase is more stable at a given temperature, it is necessary to consider the Helmholtz energies that we are able to obtain from the Luttinger-Ward functional for every solution. Previously, for the inverse temperature of $\beta = 100$, at most of the geometry points, we have identified two possible phases with different internal energies, E, that were obtained starting the iterative GF2 procedure either from an insulating or metallic solution. The results of our investigation can be found in Fig. 4 of Ref. [51]. Currently, to analyze the stability of the solutions, for a range of inverse temperatures $\beta = 25, 75, 100$, we discuss internal energy E, Helmholtz energy A, and the entropic contribution TS to the Helmholtz energy. We also improved our convergence criteria not only converging the internal energy $E = E_{1b} + E_{2b}$ (as we have done in the previous work) but also converging both the E_{1b}, E_{2b}, and the Helmholtz energy separately. This much more stringent procedure to analyze convergence of GF2 leads us to slightly revised solutions for the 1D hydrogen solid which we discuss in the subsequent sections.

The spectra are produced from analytical continuation of the imaginary axis Green's function $G(\mathbf{k}, i\omega_n)$ to the real axis $G(\mathbf{k}, \omega_n)$ [67]. The spectral weight is proportional to $\mathrm{Im}G(\mathbf{k}, \omega_n)$. A 2D color projection of the spectral function on the $(\mathbf{k}, \omega_n)$ plane can be viewed as a "correlated band structure" analogous to the conventional band structure within effective one-electron models such as Hartree–Fock and DFT. As in one-electron models, zero spectral weight at the Fermi energy ω_F is indicative of a gapped system. The peaks emerging immediately below and above ω_F for a given $\mathbf{k}$ correspond to the energies of the highest occupied (HOCO) and lowest unoccupied (LUCO) crystalline orbitals, respectively. We should stress, however, that since $G(\mathbf{k}, \omega_n)$ is a many-body correlated Green's function, such correspondence is not rigorous and merely serves as a convenient analogy.

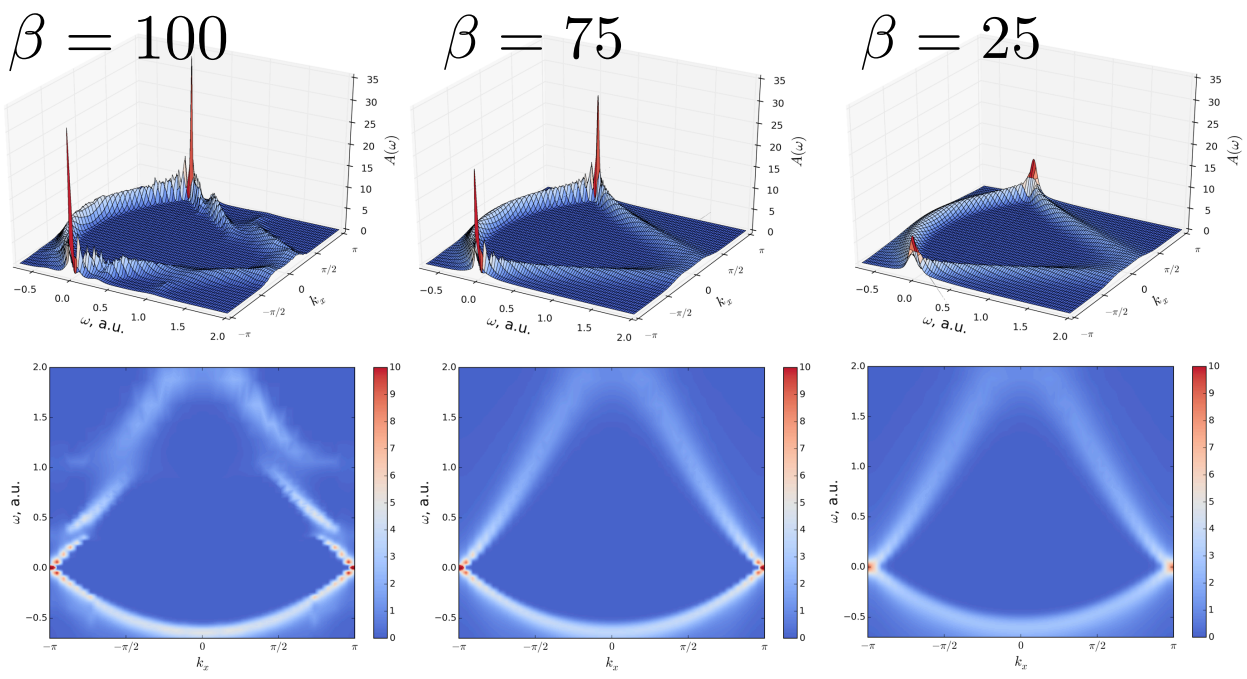

Figure 3.2: Spectral functions and projections at different inverse temperatures for the metallic solution of 1D periodic hydrogen solid at R=0.75 Å.

3.2.2.3 Short bond length/high pressure

At the interatomic separation of 0.75 Å, we recovered only one gapless, metallic solution for all the values of inverse temperature (β = 25, 75, 100). We established that starting from two different initial guesses leads in both cases to two final solutions that were different in internal energy and Helmoltz energy by less than 10^{-4} a.u. Consequently, we deemed that we obtained the same metallic solution in both cases. The spectral functions and spectral projections for this metallic solution at different values of inverse temperature are shown in Fig. 3.2. For all the temperatures examined in this short bond length regime, the self-energy displays a Fermi liquid character.

In our previous work [51], we observed a small internal energy difference between the solutions obtained using different starting point at β = 100. We currently observe that this difference can be eliminated if we assure that the convergence criteria are not only fulfilled for the total energy $E_{tot} = E_{1b} + E_{2b}$ but also both the E_{1b} and E_{2b} components separately.

β	Δ E	-T Δ S	Δ A
100	-0.00370	0.10854	0.10484
75	-0.00528	0.09971	0.09443
25	1.36×10^{-8}	-2.94×10^{-6}	-2.93×10^{-6}

Table 3.1: Thermodynamic data for a 1D periodic hydrogen solid with separation R=1.75 Å. The units for β are 1/a.u. The units for all other quantities are a.u. All values are obtained by subtracting "solution 1" from "solution 2". Δ E =E_{sol2}-E_{sol1}, Δ A =A_{sol2}-A_{sol1}, Δ S =S_{sol2}-S_{sol1}. Note that the quantities at β=25 are below the precision of convergence (1×10^{-5}).

3.2.2.4 Intermediate bond length/intermediate pressure

Spectral functions and projections for the 1D hydrogen solid with an interatomic separation of 1.75 Å are presented in Fig. 3.3. We have displayed differences in internal energy (E), entropy (written as -TΔS), and Helmholtz energy (A) in Table 3.1. For this system at the inverse temperatures of $\beta = 100$ and 75 we obtained two solutions from two different initial guesses. We are able to characterize the first solution ("solution 1") as a band insulator since the spectral function shows a gap and the self-energy displays a Fermi liquid profile. The second solution ("solution 2") is gapless and therefore a metal. At an inverse temperature of $\beta = 25$, both "solution 1" and "solution 2" obtained from two different starting guesses have the same spectra and identical Helmholtz energy, indicating that there is only one stable solution — a single phase. Note that in Fig. 3.3 for $\beta = 25$ both the spectral functions for "solution 1" and "solution 2" seem to have different heights; however, it is an illusion since both spectral functions are plotted with a different z-axis range. We deem that the Helmholtz energy is identical for both these solutions at $\beta = 25$ since the obtained differences are below our convergence threshold which is 1×10^{-5} a.u.

For two lower temperatures ($\beta = 100$ and 75) by comparing thermodynamic quantities, we are able to determine which phase, "solution 1" or "solution 2", is the most thermodynamically stable. From the data in Table 3.1, we are able to determine that "solution 1" is the most stable phase from the positive value of ΔA at both β=100 and β=75. It is also interesting to note, that this solution is stable due to the entropic factor not due to the difference in the internal energy.

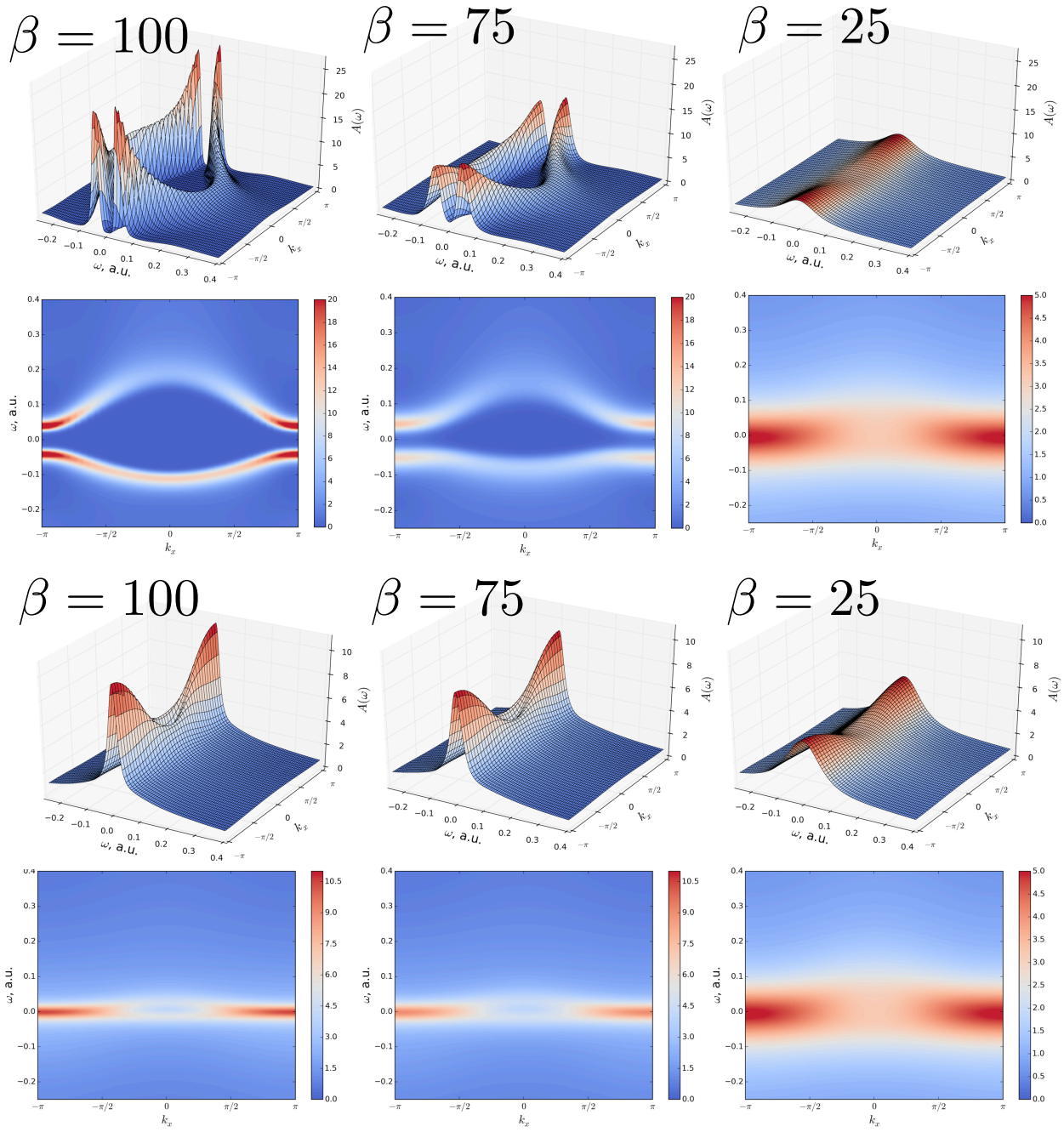

Figure 3.3: Spectral functions and projections at different inverse temperatures for the band insulator ("solution 1") and the metallic solution ("solution 2") of 1D periodic hydrogen solid at R=1.75 Å. Note the difference in scale between "solution 1" and "solution 2".

β	Δ E	-T Δ S	Δ A
100	0.08489	0.16257	0.24746
75	0.07103	0.16155	0.23259
25	6.09×10^{-8}	2.96×10^{-5}	2.97×10^{-5}

Table 3.2: Thermodynamic data for a 1D periodic hydrogen solid with separation R=2.5 Å. The units for β are 1/a.u. The units for all other quantities are a.u. All values are obtained by subtracting "solution 1" from "solution 2". Δ E =E_{sol2}-E_{sol1}, Δ A =A_{sol2}-A_{sol1}, Δ S =S_{sol2}-S_{sol1}. Note that the quantities at β=25 are below or comparable with the precision of convergence (1×10^{-5}).

3.2.2.5 Long bond length/low pressure

Similar to the R=1.75 Å regime, for an interatomic separation of 2.5 Å at inverse temperatures β = 100 and 75, we recover two solutions from the two different initial guesses, see Fig. 3.4. At a high temperature β=25 we observe only one solution independent of the initial guess, and thus only a single phase is present. From the positive value of ΔA we are able to see that "solution 1" is the most stable phase at β=75 and β=100 (Table 3.2). This solution is a band insulator since it has a Fermi liquid self-energy profile at these temperatures. The other solution, denoted as "solution 2" at low temperature is metallic and changes into a Mott insulator at high temperatures. The internuclear distance of R=2.5 Å is close to the region where the phase transition occurs, thus results obtained from GF2 which is a low order perturbation expansion may not be reliable. The low level perturbation theories such as GF2 are known to be more accurate deep within a phase and can experience problems near the phase transition point.

Finally, at an interatomic separation of R=4.0 Å, for all the temperatures, both initial guesses yield the same converged GF2 result - a single phase. The spectra as a function of inverse temperature can be seen in Fig. 3.5. This single solution is a Mott insulator as confirmed by the divergent imaginary part of the self-energy.

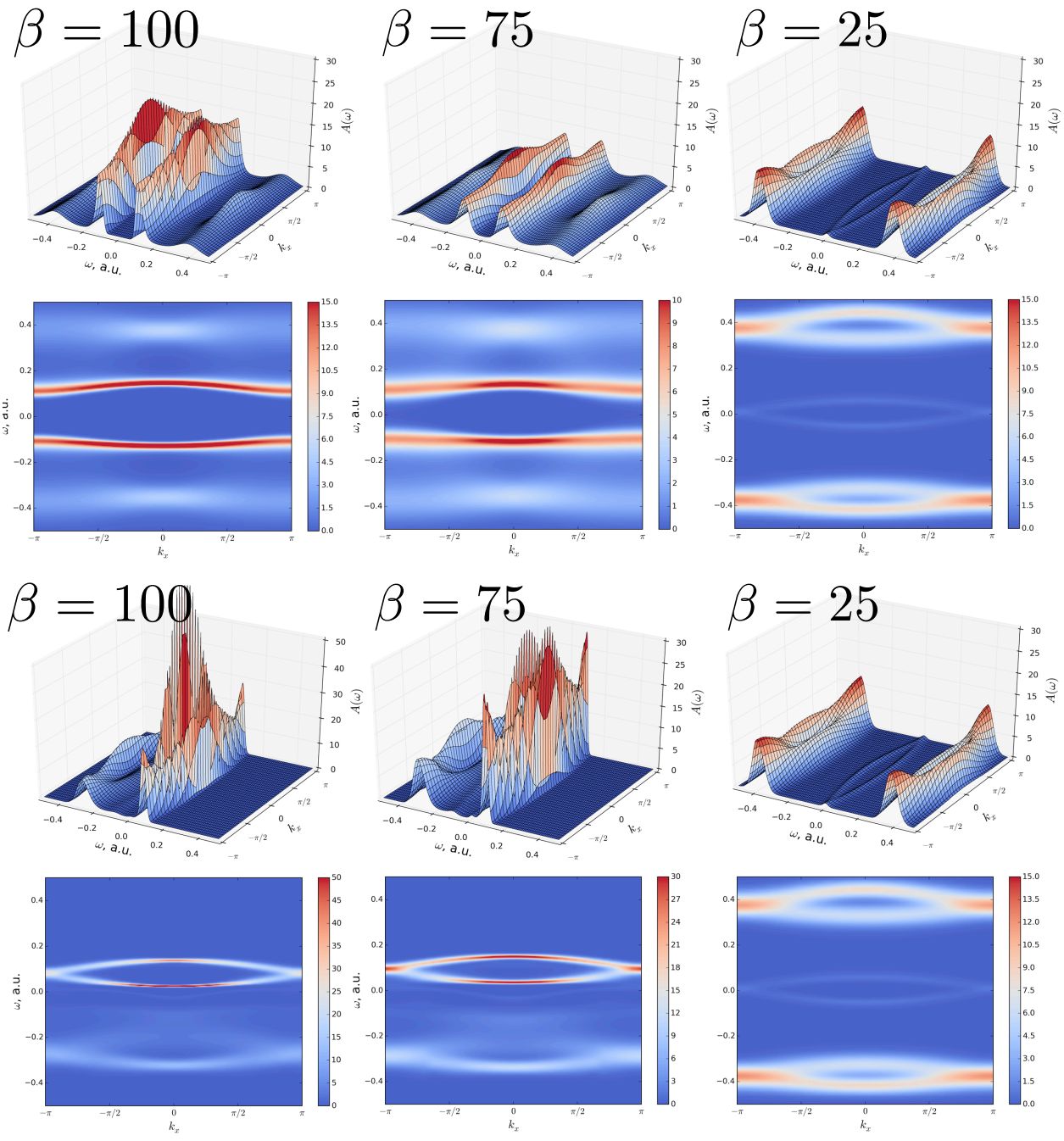

Figure 3.4: Spectral functions and projections at different inverse temperatures for the band insulator ("solution 1") and the metallic solution ("solution 2") of 1D periodic hydrogen solid at R=2.5 Å.

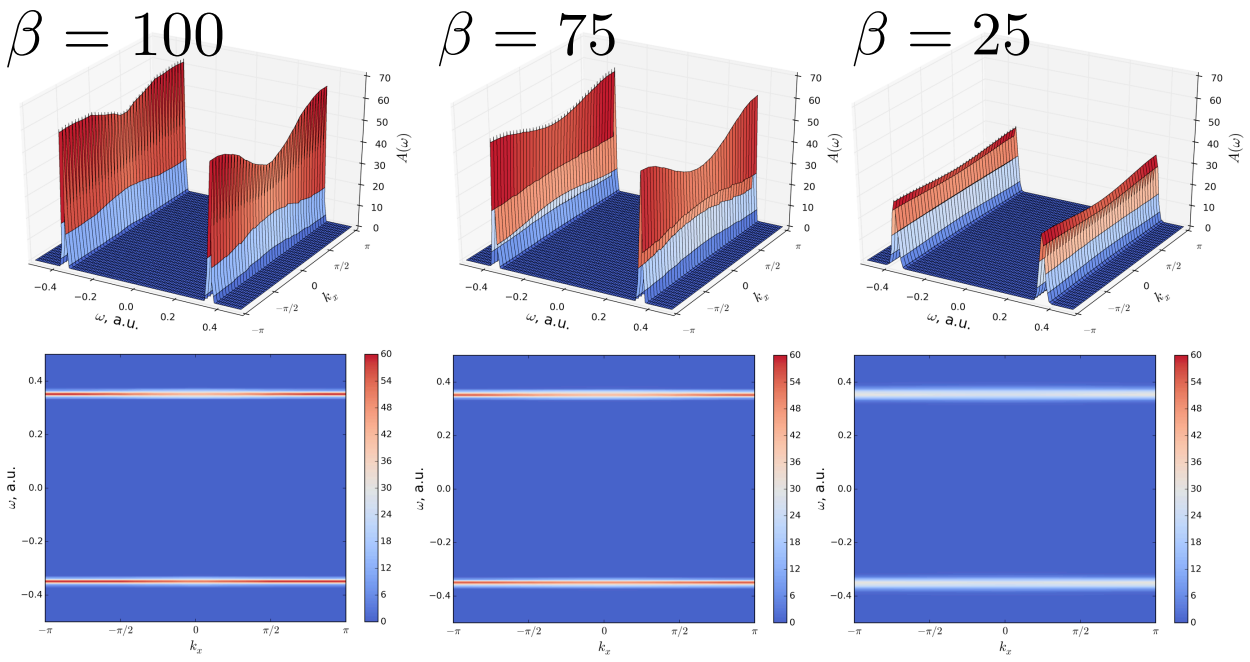

Figure 3.5: Spectral functions and projections at different inverse temperatures for the Mott insulator present in 1D periodic hydrogen solid at R=4.0 Å.

3.2.2.6 GF2 phase diagram for 1D hydrogen solid

It is instructive now to collect all the data and construct a simple phase diagram for the 1D hydrogen solid as a function of inverse temperature β and intermolecular distance R. We have plotted the phase diagram in Fig. 3.6. On this diagram, for these regions where two phases coexist, we denoted the most stable phase according to the Helmholtz energy A by framing its symbol using a black line.

For the shortest bond length (R=0.75 Å), the 1D hydrogen solid remains metallic at all temperatures considered and only one phase is present. At intermediate bond lengths (R=1.75, 2.0 Å), multiple phases coexist. At lower temperatures, we recover both a metal and band insulator as possible solutions, with the band insulator being the most stable phase according to the Helmholtz energies. This is in line with physical intuition that we should recover an insulator rather than a metal at low temperature. For R=1.75 Å, at temperatures higher than $\beta = 50$, we recover only the metallic phase.

For R=2.0 Å at high temperature (β = 25), we see both a metal and a Mott insulator coexisting, with the Mott insulator being the most stable phase. At lower temperatures, we see the coexistance of a metallic and band insulator solution. The Helmholtz energy indicates that band insulator is the most stable phase.

At a longer bond length of (R=2.5 Å), multiple phases are still present. As in the cases of intermediate bond length, we recover both a band insulator and a metal solution, with Helmholtz energy favoring the band solution. We would like to reiterate that a phase transition occurs somewhere in this intermediate region, and it is likely that the results of a second-order perturbation theory may not be accurate enough. At higher temperatures, we recover a Mott insulator as the only phase present.

For the largest separation (R=4.0 Å), the system remains a Mott insulator at all studied temperatures.

3.2.2.7 Periodic calculation of 1D boron nitride

In this section we present a periodic calculation of 1D boron nitride (BN) at inverse temperatures β =70, 75, and 100. The B–N distance is set to 1.445 Å, the bond length in the corresponding 2D system [68]. For these calculations we used a modification of the ANO-pVDZ Gaussian basis set [69] from which, in order to avoid linear dependencies, we removed the diffuse (below 0.1) exponents and polarization functions. Larger grids of 30000 Matsubara frequencies and 100 Legendre polynomials were found necessary for an adequate discretization for the self-energy and Green's function. The self-energy is evaluated encompassing 39 cells — as many as needed for a converged Hartree–Fock exchange.

Shown in Fig. 3.7 is the spectral projection of the real-frequency correlated Green's function at β=100. Using the analogy previously discussed at the end of Section V. B, we plot the "highest occupied" and "lowest unoccupied correlated bands" of 1D BN separated by a sizable gap of approximately 3.5 eV at k=-π. This magnitude of the band gap is expected based on the properties of its 2D counterpart [68].

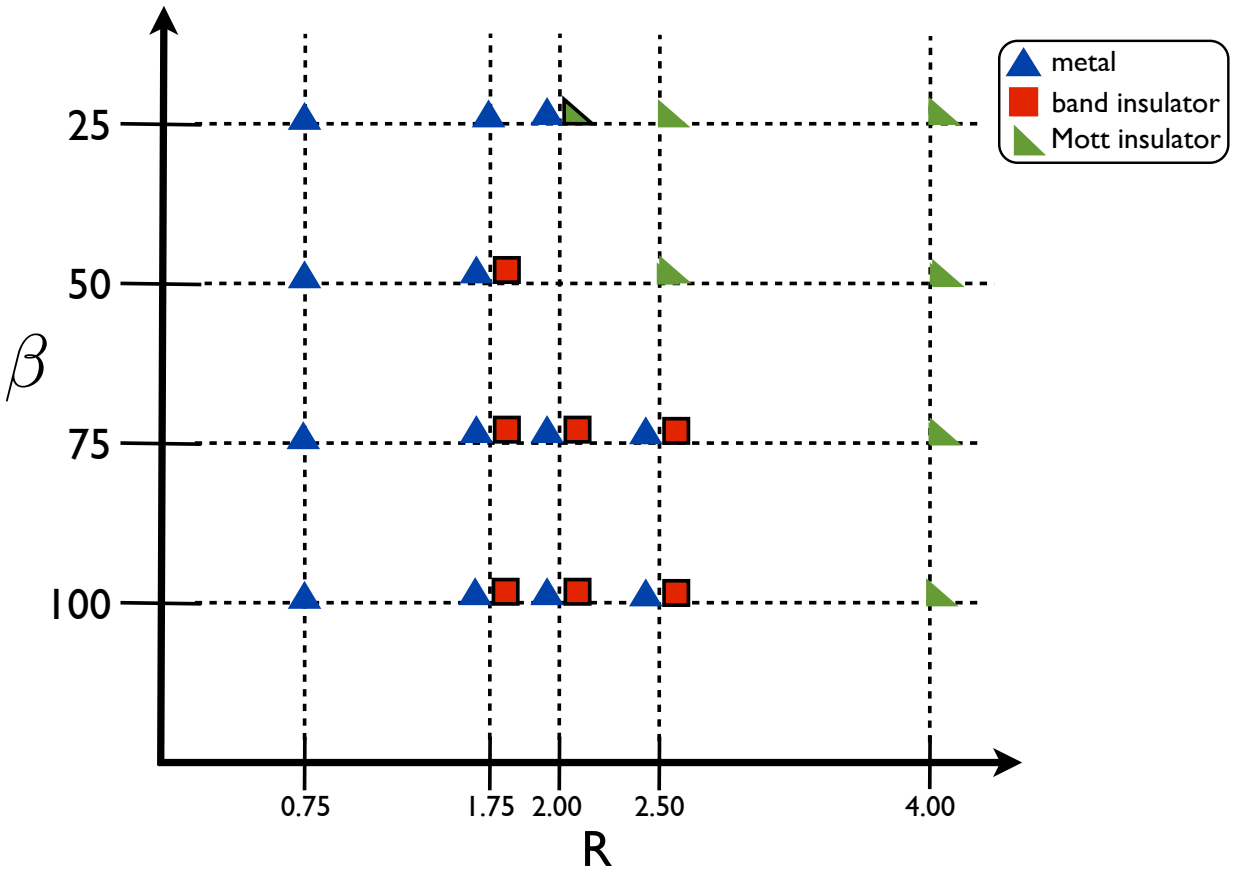

Figure 3.6: A phase diagram containing all distances and temperatures calculated for a 1D hydrogen solid. Where multiple phases exist, the most stable phase is outlined in black. β is inverse temperature in units 1/a.u. and R is the separation between hydrogens in Å.

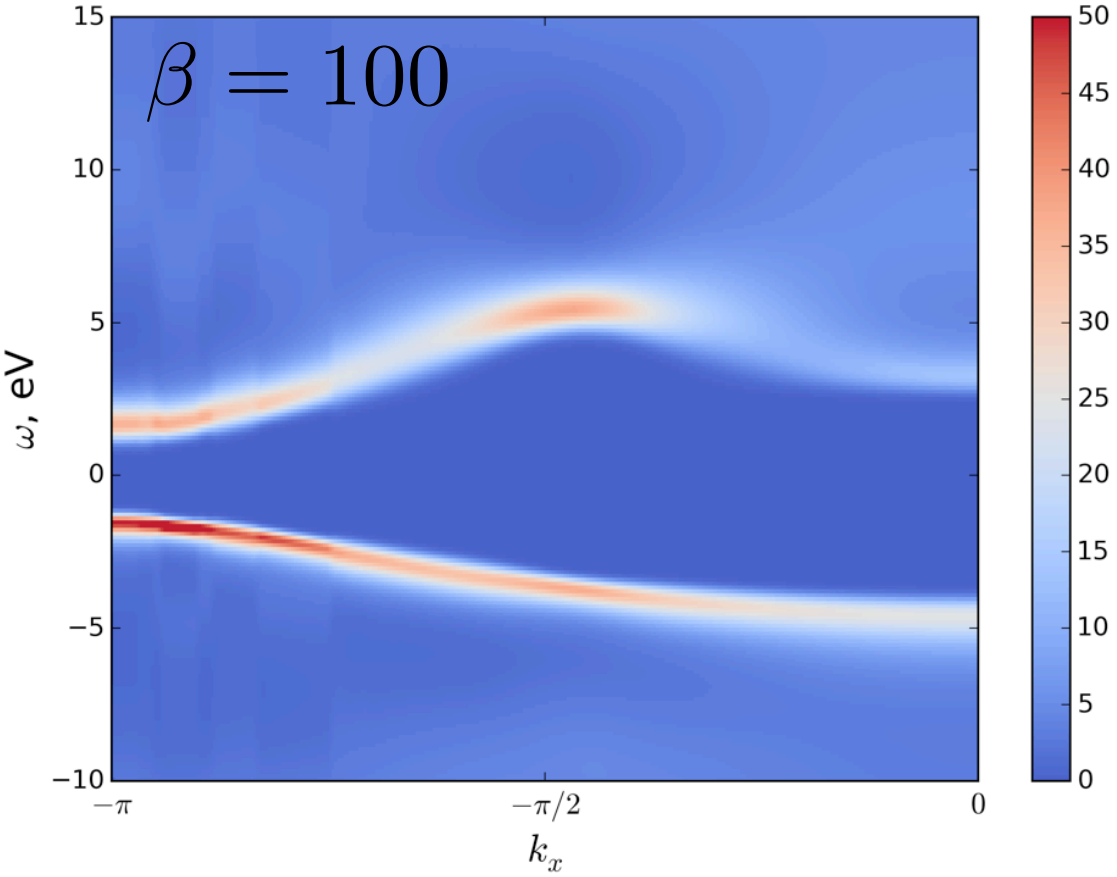

Figure 3.7: Spectral projection in the vicinity of the Fermi energy at β=100 of periodic 1D boron nitride solid. Only the "correlated bands" corresponding to the conventional HOCO's and LUCO's (see Sec. V. B) are displayed. Note that the energy scale is in eV.

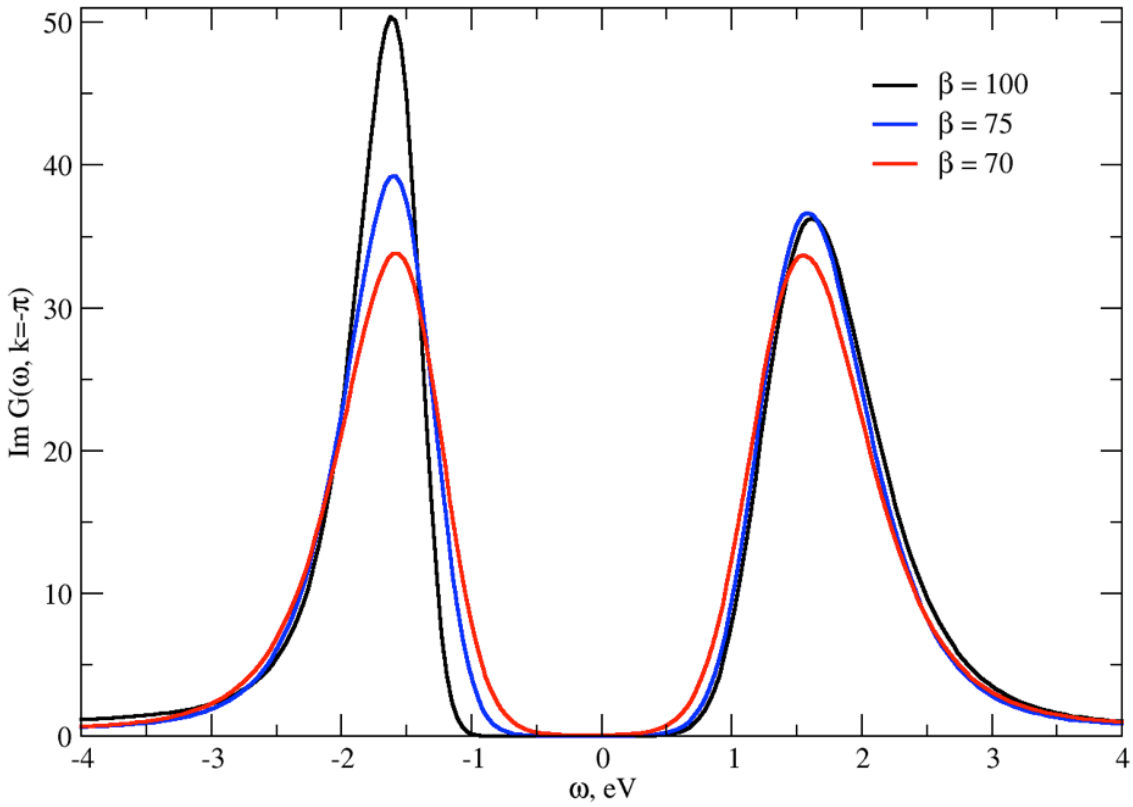

Figure 3.8: Periodic 1D boron nitride solid spectrum for the "correlated HOCO and LUCO" (see Sec. V. B) for several temperatures at k=$-\pi$. The chemical potential was adjusted for $\omega = 0$ to fall in the middle of the band gap.

Once again, we treat such a simple system as a benchmark example and we are interested in the evolution of the 1D BN band gap as the temperature changes and influences electronic degrees of freedom. Let us stress that while an evolution of the spectrum as a function of temperature is expected, in order to reproduce it reliably, the computational procedure must be very robust. We not only must be able to iteratively converge Green's function and self-energy yielding different Green's functions at different temperatures, we also must continue the results obtained on the imaginary axis to the real axis risking that the continuation will obscure the spectral features and the gap temperature dependence will no longer be visible.

In Fig. 3.8 we plot the spectrum at k=-π for β=100, 75, and 70. As expected, with the increase of temperature (decrease of β) the spectral peaks corresponding to the bands broaden and the band gap reduces. Note that both Fig. 3.7 and 3.8 use eV as energy units for clarity.

3.2.3 Conclusion

While the theory describing the connection between the Matsubara Green's function formalism and thermodynamics has been known since the 1960s, few computational methods are currently capable of employing the Matsubara formalism for realistic systems. This is due to its computationally demanding nature that requires complicated time and frequency grids as well as the iterative nature of the equations. Moreover, little is know about obtaining different solutions corresponding to different phases or non-physical solutions that can appear as the result of the non-linear procedure used when Green's functions are constructed iteratively on the imaginary axis.

In our last work [51], we have demonstrated one of the first applications of the fully self-consistent Matsubara Green's function formalism to a benchmark periodic problem with realistic interactions, that is, a 1D hydrogen solid. In the current work, we have shown that it is possible to evaluate temperature dependent thermodynamic quantities using a self-consistent second-order Green's function method. Using the self-consistent Green's function and self-energy, we were able to evaluate the Luttinger-Ward functional at various temperatures and obtain static thermodynamic quantities such as Helmholtz energy, internal energy, and entropy. Evaluation of these quantities

gives us access to the partition function and any thermodynamic quantity that can be derived from it. Unlike the FCI case, in GF2 we do not need to explicitly calculate excited state energies or Boltzmann factors, making calculation of thermodynamic quantities for larger systems feasible.

To calibrate the thermodynamic data obtained from GF2 against FCI, we have illustrated that for a hydrogen fluoride molecule at high temperature, we are able to obtain energies in excellent agreement with finite temperature FCI. In the lower temperature regime, we observed, as expected, some deviation from the FCI answer but the overall quality of the results still remained high.

Finally, since the thermodynamic data can be used to construct phase diagrams, we used a simple 1D hydrogen solid to investigate possible phases at different temperatures and interatomic distances. We obtained different phases such as a band insulator, Mott insulator, or metal, and we were able to distinguish which phase is more stable at various temperatures. Determining the stability is possible due to our ability to calculate not only the internal energy but also the entropic contribution at each temperature. Consequently, based on the difference of the Helmholtz energy, we are able to determine the most stable phase for each of the temperature points.

Additionally, we have performed a calculation of 1D periodic BN solid demonstrating that GF2 can reproduce the gap deviation as a function of temperature. Thus, for higher temperatures, we have observed the narrowing of the electronic bandgap.

While we acknowledge that GF2 is a low order perturbative method and as such can deliver results that are inaccurate, we believe that for most weakly and moderately correlated systems such as semiconductors with small band gaps, it can be used in the future to provide accurate thermodynamic data and phase diagrams. For systems where the correlations are strong, GF2 can be combined with methods such as self-energy embedding theory (SEET) [53, 70, 71] to provide accurate answers concerning thermodynamics.

3.2.4 Appendix: High-frequency expansion of the Green's function for evaluating the Luttinger-Ward functional

Here, we consider the contribution to the Luttinger-Ward functional in the high frequency limit. In the Matsubara formalism for large frequencies, the Green's function and self-energy can be expressed as a series

$$G(i\omega_n) = \frac{G_1}{i\omega_n} + \frac{G_2}{(i\omega_n)^2} + O(\frac{1}{(i\omega_n)^3}), \tag{3.24}$$

$$\Sigma(i\omega_n) = \frac{\Sigma_1}{i\omega_n} + \frac{\Sigma_2}{(i\omega_n)^2} + O(\frac{1}{(i\omega_n)^3}). \tag{3.25}$$

The coefficients for the Green's function expansion for non-orthogonal orbitals with a quantum chemistry Hamiltonian [72] are given as

$$\begin{aligned} G_1 &= S^{-1}, \\ G_2 &= S^{-1}(F - \mu S)S^{-1}. \end{aligned} \tag{3.26}$$

The Σ_1 and Σ_2 coefficient of the self-energy has a complicated explicit form as demonstrated in Ref. rusakov2014local and is evaluated numerically as

$$\begin{aligned} \Sigma_1 &= \mathrm{Re}\left(\Sigma(i\omega_{max}) \times i\omega_{max}\right) \\ \Sigma_2 &= \left(\Sigma(i\omega_{max}) - \frac{\Sigma_1}{i\omega_{max}}\right) \times (i\omega_{max})^2. \end{aligned} \tag{3.27}$$

For the molecular example used in this work, the high frequency contribution to Tr[$G\Sigma$] was evaluated in the same manner as previously discussed in Ref. GF2,spline. At the very high temperatures considered for molecular examples, the high frequency contribution becomes negligible. However, it is necessary to include at the lower temperatures considered. The high-frequency contribution to the $\Omega^k_{Tr[G\Sigma]}$ term of Eq. 3.19 can be evaluated in a way analogous to the molecular

	Internal Energy (a.u.)			Grand Potential (a.u.)			Entropy (k_B)		
T (K)	Hartree-Fock	GF2	FCI	Hartree-Fock	GF2	FCI	Hartree-Fock	GF2	FCI
10^3	-98.571	-98.588	-98.597	-98.571	-98.585	-99.845	0.0	-0.003	0.0
10^4	-98.571	-98.588	-98.597	-98.571	-98.621	-99.944	0.0	0.0	0.0
10^5	-97.944	-98.135	-98.049	-101.021	-103.067	-102.107	3.175	3.566	3.475
10^6	-96.794	-96.988	-96.945	-150.563	-151.410	-151.244	4.979	4.949	4.958
10^7	-92.028	-92.057	-92.056	-729.937	-730.100	-730.095	5.348	5.348	5.348
10^8	-88.483	-88.487	-88.487	-6846.975	-6847.001	-6847.003	5.406	5.406	5.406

Table 3.3: FCI, GF2, and finite temperature Hartree-Fock results for the hydrogen fluoride molecule in STO-3G basis. A higher value of temperature corresponds to a smaller value of $\beta = 1/k_B T$. Note that the grand potential depends on chemical potential $\Omega = E - TS - \mu N$ that for gaped system is not uniquely defined. The difference in the FCI, finite temperature Hartree-Fock, and GF2 for the $10^4 - 10^4$ K temperatures are the result of this non-uniqueness of the chemical potential. The Helmholtz energy $A = \Omega + \mu N = E - TS$, which is the sum of the grand potential and μN term does not suffer from this non-uniqueness.

case.

To evaluate the high frequency contribution to the logarithm term Tr[ln{$1 - G\Sigma$}] in Eq. 3.17, we expanded the logarithm as a Taylor series $\ln(1 - x) = x - \frac{x^2}{2} + \ldots$ to yield

$$\ln\Big(1 - \frac{G_1\Sigma_1}{(i\omega_n)^2}\Big) = \frac{G_1\Sigma_1}{(i\omega_n)^2} + O\Big(\frac{1}{(i\omega_n)^3}\Big). \tag{3.28}$$

We exclude in this expansion all terms that are equal or smaller in magnitude than $O\Big(\frac{1}{(i\omega_n)^3}\Big)$. Thus, it is only necessary practically to evaluate the first term in the expansion to capture the important contribution from the high frequency limit. We would like to emphasize that although we do not present results including the high frequency contribution to the logarithm term Tr[ln{$1 - G\Sigma$}] in Eq. 3.17 for the periodic hydrogen solid, this term was evaluated and was found to be minuscule compared to the magnitude of the other energies. However, we would like stress that it is possible that this contribution may be substantial for other systems.

CHAPTER 4

Spectra

4.1 Introduction

A crucial aim of electronic structure has been to provide theoretical insight to experiments through calculation of ionization potentials (IP) and electron affinities (EA). While ab-initio methods contain information related to these spectroscopic quantities, they are not always able to produce reliable chemical accuracy for the system under investigation. Additionally, even if an electronic structure method is known to be accurate or reliable, the IPs and EAs are not always straightforward to obtain. Computational cost produces an additional barrier, making some methods only applicable to small systems with modest basis sets.

Beginning from Koopmans' theorem [73], several schemes have been invented and used to extract IPs and EAs from wavefunction electronic structure methods. There are several excellent studies detailing the use and limitations of these methods, and it is clear that such schemes have provided invaluable insight that has advanced both experimental and theoretical physical chemistry. Similar formulations have employed the use of density functional theory (DFT) and there are a number of studies outlining the theoretical and practical aspects of such an approach. A recent series of papers conducts a systematic study of many of these methods for a set of small organic molecules. [74, 75, 76, 77] While both of these methods are viable and used in the quantum chemistry community, there is no standout method for obtaining these quantities for systems of appreciable size.

Calculating accurate ground state properties of molecules has historically been a huge aim of electronic structure calculations for chemists. Therefore, it is acceptable that wavefunction and DFT methods carry out calculations at zero-temperature. However, to make reliable physical comparisons with experiments, which are carried out at non-zero temperature, it is necessary to incorporate temperature into the calculation of spectral quantities. While wavefunction and DFT methods have finite-temperature extensions of the zero-temperature formalism, they are not used frequently in the evaluation of spectra. Furthermore, these implementations are usually more costly than the parent zero-temperature methods. For these reasons, we seek an electronic structure method to calculate spectra that incorporates temperature and can be applied to realistic chemical systems.

In addition to wavefunction and DFT methods, quantum chemists have employed the zero-temperature Green's function to study electronic structure and produce spectroscopic quantities.[78] Although the poles of the zero-temperature Green's function are the IPs and EAs of the system, giving this method a clear connection with spectroscopy, computational limitations have made its use less attractive than wavefunction or DFT methods. Storage requirements and mathematical considerations make can make this method more cumbersome to employ to obtain ground state energies than other well established black-box electronic structure methods.

The finite-temperature (Matsubara) Green's function method is not an extension of a zero-temperature method, but is developed under a separate formalism, capable of producing different quantities. The mathematical structure of the Green's function differs from that at zero-temperature in that it no longer has poles corresponding to IPs and EAs. In losing this information, we gain the advantage of the Green's function now being a smooth function that can be evaluated iteratively in a self-consistent manner. This allows us to evaluate the finite-temperature Green's function at a reasonable computational cost using a second-order approximation to the self-energy (GF2) that can be employed in a black-box manner [50]. While the Green's function contains information about the spectra, the finite-temperature method no longer provide such straightforward access to the IPs and EAs as the zero-temperature method. It is challenging to analytically continue the

imaginary Green's function to the real axis to resolve the details of the spectrum. Therefore, when investigating methods to obtain IPs and EAs from the imaginary frequency axis, it is crucial to evaluate the robustness of such procedures.

In this work, we describe procedures to extract IP/EA from a finite-temperature Green's function, and demonstrate how reliably one is able to produce such quantities. We calculate systems with known IPs/EAs from experiment and for which highly accurate calculated values are available. Further, we apply these methods to larger systems (DNA/RNA bases) to illustrate the applicability of these methods to chemically interesting species. We calculate singlet-triplet gaps of several molecules using GF2, to illustrate that this method can give reasonable values for these quantities as well. The purpose of this study is to systematically test the behavior of various ways to obtain the IPs and EAs from an imaginary Green's function and is not meant to compete in chemical accuracy with high level theories. Instead, we aim to understand how reliably one may obtain IPs and EAs from the temperature-dependent Green's function, which was only carried out for a few atoms and small molecules in the past[18, 19, 20].

We begin by investigating a method to obtain IPs and EAs *directly* from the imaginary axis, known as the Extended Koopmans' Theorem (EKT). This is a simple eigenvalue procedure that is an extension of Koopmans' Theorem from Hartree-Fock. We then investigate methods that are carried out *partially* on the imaginary axis, beginning from the density matrix of a converged GF2 calculation. From this converged density matrix, we are able to construct a Green's function in real frequency, giving direct access to the spectra.

We show that different procedures of evaluation of spectral quantities, even at the same level of theory, can yield values for IPs and EAs which can vary by several electron volts. We conclude that one must exercise caution when choosing a procedure to evaluate IP and EA, even for the same system at the same level of theory, in order to make reliable comparisons.We show that quantities obtained directly from the imaginary axis are unreliable in general, while the quantities obtained partially on the real axis are more consistent, reiterating that it is nontrivial to obtain real axis information from an imaginary axis Green's function.

This chapter is organized as follows. In Section 4.2 we describe the details of our perturbative second-order Green's function method, GF2, which is calculated on the imaginary axis. We follow in Section 4.3 with descriptions of the various procedures used to obtain the IPs, EAs, and fundamental gaps using our GF2 implementation.

4.2 GF2: An imaginary axis formulation

In any correlated system described using Green's function language, the self-energy, $\mathbf{\Sigma}(i\omega_n)$, accounts for many-body correlation static and dynamic effects and it can be evaluated using the Dyson equation

$$\mathbf{\Sigma}(i\omega_n) = \mathbf{G_0}(i\omega_n)^{-1} - \mathbf{G}(i\omega)^{-1}. \tag{4.1}$$

The non-interacting Green's function, $\mathbf{G_0}(i\omega_n)$, is expressed as

$$\mathbf{G_0} = [(i\omega_n + \mu)\mathbf{S} - \mathbf{F}]^{-1}, \tag{4.2}$$

where $i\omega_n = \frac{(2n+1)i\pi}{\beta}$ are imaginary (Matsubara) frequencies forming a grid for the Green's function evaluation. The inverse temperature is denoted as β, the chemical potential is μ, the overlap and Fock matrices are denoted as $\mathbf{S}$ and $\mathbf{F}$, respectively.

In the self-consistent Green's function, the self-energy is evaluated self-consistently and approximated at the second order as

$$\begin{aligned}\Sigma^{(2)}_{ij}(\tau) = -\sum_{klmnpq} & G_{kl}(\tau)G_{mn}(\tau)G_{pq}(-\tau)\times \\ & \times v_{ikmq}(2v_{ljpn} - v_{pjln})\end{aligned} \tag{4.3}$$

where v_{ijkl} are the two-electron integrals in the atomic orbital (AO) basis in the chemist's notation, and τ is an imaginary time.

Since the GF2 Green's function and self-energy are evaluated on the imaginary axis they are

smooth antiperiodic functions. This is advantageous since it allows us to iterate the GF2 self-consistent equations until the convergence is reached, where the self-energy, $\mathbf{\Sigma}[\mathbf{G}]$, and Fock matrix $\mathbf{F}[\mathbf{G}]$ are both functionals of Green's function. The iterations are much more difficult to execute when the Green's function and self-energy is evaluated on the real axis since then Green's function contains multiple peaks corresponding to IPs and EAs of the system. Consequently, in order to solve the equations iteratively one would need to use an adaptive grid and shift the Green's function poles during iterations [79]. The ease of iterating is one of the reasons why imaginary axis formulation of Green's function methods is advantageous. Since the calculation can be started from the HF or DFT Fock matrix, the"memory" of the starting point can be removed during the iterations, making the whole calculation reference independent. This is in contrast to partially self-consistent methods such as G_0W_0, which show a clear dependence on the starting value [80].

During the GF2 calculation, the Fock matrix and the self-energy are updated iteratively. The Fock matrix $\mathbf{F}[\mathbf{P}]$ is updated throught the density matrix $\mathbf{P}$ updates evaluated from Green's function as $\mathbf{P} = -2\mathbf{G}(\tau = \beta)$. Consequently, since the Fock matrix depends on the density matrix that is a static, frequency independent quantity, we expect that the final converged Fock matrix should be independent if the iterative procedure is being carried out on the real or imaginary axis. This would suggest that perhaps instead of very difficult iterating Green's function equations on the real axis until self-consistency, one could first do the "easy iterations" on the imaginary axis to obtain $\mathbf{F}[\mathbf{P}]$ and then perform a couple of iterations to evaluate $\mathbf{\Sigma}[\mathbf{G}]$ while keeping the Fock matrix fixed.

In the next section, we will consider several schemes that will allow us to evaluate spectral quantities while fully or partially using the information that is evaluated on the imaginary axis, avoiding very difficult real axis iterations.

4.3 Fundamental Gap Evaluation for GF2

In this section, we will discuss various methods that we used to obtain IP and EA. These can be used to obtain the fundamental gap. The first method, the Extended Koopmans' Theorem (EKT)

involves obtaining the IP and EA *directly* from the imaginary axis formalism. The other methods, which we call, (F(GF2)+$\Sigma^{(2)}$, HF+ $\Sigma^{(2)}_{ii}$, and HF + iter $\Sigma^{(2)}_{ii}$) require a "single iteration" of Green's function theory on the real axis, and therefore necessitate one to build the self-energy on the real frequency axis. In all cases, we begin from the converged density matrix and Fock matrix obtained from GF2 calculations on the imaginary axis.

4.3.1 Extended Koopmans' Theorem

The extended Koopmans' theorem (EKT) provides a straightforward way to calculate IPs and EAs directly from the imaginary axis Green's function.

A system of interest is described by Hamiltonian $\hat{H}$ and its wave function is an N electron state $|N\rangle$. The energy of this systems is given by $\hat{H}|N\rangle = E|N\rangle$. The $(N-1)$ and $(N+1)$ wave function can be obtained by acting on the N-electron state with the second-quantized operators, $\hat{a}|N\rangle = |N-1\rangle$, $\hat{a}^\dagger|N\rangle = |N+1\rangle$. Consequently, the energies of the anion, neutral, and cation states can be expressed as

$$\begin{aligned} E_{N+1} &= \langle N|\hat{a}\,\hat{H}\,\hat{a}^\dagger|N\rangle\,, \\ E_N &= \langle N|\hat{H}|N\rangle\,, \\ E_{N-1} &= \langle N|\hat{a}^\dagger\,\hat{H}\,\hat{a}|N\rangle\,, \end{aligned} \tag{4.4}$$

respectively. Given Eq. 4.4, IP and EA can be defined as

$$\begin{aligned} IP &= E_{N-1} - E_N = -\langle N|\hat{a}^\dagger[\hat{a},\hat{H}]|N\rangle\,, \\ EA &= E_N - E_{N+1} = \langle N|\hat{a}[\hat{a}^\dagger,\hat{H}]|N\rangle\,. \end{aligned} \tag{4.5}$$

It should be understood these operators are expanded in a basis, $\hat{a} = \sum_i c_i\hat{\phi}_i$, with the expansion coefficients c_i chosen so that the anion (cation) state remains normalized [81].

For practical calculations we want to connect Eq. 4.5 to the quantities such as $G(\tau)$ that can be evaluated in Green's function many-body theory [11]. This connection can be realized in the following way

$$\lim_{\tau\to 0}\frac{\partial G(\tau)}{\partial \tau} = \begin{cases} \langle N|\hat{a}[\hat{a}^\dagger, \hat{H}]|N\rangle\,, & \tau > 0 \\ \langle N|\hat{a}^\dagger[\hat{a}, \hat{H}]|N\rangle\,, & \tau < 0. \end{cases} \tag{4.6}$$

The above equation implies that to evaluate the IP and EA, we must solve the following equations

$$\mathbf{H}^I\mathbf{c} = \epsilon\mathbf{P}\mathbf{c} \tag{4.7}$$

$$\mathbf{H}^A\mathbf{c} = \epsilon\mathbf{P}_v\mathbf{c}, \tag{4.8}$$

where $\mathbf{H}^I$ and $\mathbf{H}^A$ refer to matrices that we will call generalized Fock matrices that are defined as $[\mathbf{H}^I]_{ij} \equiv \langle N|\hat{\phi}_i^\dagger[\hat{\phi}_j, \hat{H}]|N\rangle$ and $[\mathbf{H}^A]_{ij} \equiv -\langle N|\hat{\phi}_i[\hat{\phi}_j^\dagger, \hat{H}]|N\rangle$. The "particle" and "hole" density matrices are denoted as $\mathbf{P}$ and $\mathbf{P}_v$.

In wave function methods, the evaluation of the $\mathbf{H}^I$ and $\mathbf{H}^A$ matrices is a major task, however, in the many-body Green's function methods they can be evaluated simply as time-derivatives of the Green's function on the imaginary-domain in the AO basis, as shown in Eq. 4.6. For compactness, we simply denote these two possibilities as $\partial_\tau G(\tau)|_{0^+}$ and $\partial_\tau G(\tau)|_{0^-}$.
Due to the discontinuity of the Green's function at $\tau = 0$, Eq. 4.6 has its two branch form. Furthermore since $G(\tau) = -G(\tau + \beta)$, the partial derivatives can be expressed as $\partial_\tau G(\tau)|_{0^-} = -\partial_\tau G(\tau)|_\beta$.

The Eqs. 4.7-4.8 can be written in an eigenvalue form by introducing $\mathbf{c}' = \mathbf{P}^{1/2}\mathbf{c}$ and $\mathbf{c}' = \mathbf{P}_v^{1/2}\mathbf{c}$ while multiplying on the left by $\mathbf{P}^{-1/2}$ and $\mathbf{P}_v^{-1/2}$, respectively. Consequently, we will obtain

$$\Delta_- = 2\mathbf{P}^{-1/2}\partial_\tau\mathbf{G}(\tau)|_{0^-}\mathbf{P}^{-1/2}, \tag{4.9}$$

$$\Delta_+ = -2\mathbf{P}_v^{-1/2}\partial_\tau\mathbf{G}(\tau)|_{0^+}\mathbf{P}_v^{-1/2}, \tag{4.10}$$

where the eigenequations yielding IP and EA are

$$\Delta_{-}\mathbf{c}' = \epsilon_I \mathbf{c}' \ , \ \epsilon_I = IP + \mu \tag{4.11}$$

$$\Delta_{+}\mathbf{c}' = \epsilon_A \mathbf{c}' \ , \ \epsilon_A = EA + \mu. \tag{4.12}$$

The factors of two in Eqs. 4.9-4.10 account for double occupation in our spin-restricted formalism. Note that if we were to substitute $\mathbf{G}(\tau)$ with the Hartree-Fock Green's function $\mathbf{G}^{\mathrm{HF}}(\tau)$, the eigenvalues of Eq. 4.12 are the Koopmans' theorem eigenvalues.

One subtlety is that diagonalizing $\Delta_{\pm}$ will of course yield as many eigenvalues as there are AO basis functions, N_b, yet only some of these eigenvalues will be physically meaningful as IPs or EAs. The simplest way to identify the correct eigenvalues is by the analyzing the Dyson occupations which are the diagonal elements of $\mathbf{D}$ and $\mathbf{D}_v$ matrices defined as

$$\begin{aligned} \mathbf{C}_{-}^{\dagger}\mathbf{P}\,\mathbf{C}_{-} &= \mathbf{D}, \\ \mathbf{C}_{+}^{\dagger}\mathbf{P}_v\mathbf{C}_{+} &= \mathbf{D}_v, \end{aligned} \tag{4.13}$$

where $\mathbf{C}_{\pm}$ are the matrices of eigenvectors, $\mathbf{C} = \{\mathbf{c}_1^{'}, \mathbf{c}_2^{'}, \ldots\}$, obtained from diagonalizing $\Delta_{\pm}$. Note that the diagonal elements of $\mathbf{D}$ correspond to the Dyson orbital occupations in the electron removal process while the diagonal elements of $\mathbf{D}_v$ are the Dyson orbital occupations in electron attachment process.

We would like to mention that the use of the extended Koopmans' theorem is not limited to GF2 or even Green's function methods. In the past it has been applied to a variety of cases at different levels of theory [82, 83, 84, 85, 86, 87, 88, 89, 90, 91].

The results from applying EKT to the GF2 Green's function will be listed in Sec. 4.4.

4.3.2 HF+$\Sigma^{(2)}_{ii}$ and HF+iter $\Sigma^{(2)}_{ii}$

Here, we describe the procedure to evaluate the second-order self-energy on the real axis, starting with the converged Fock matrix **F** obtained from our GF2 procedure iterated on the imaginary axis. The real axis self-energy is expressed as

$$\Sigma^{(2)}_{ij}(\omega_n) = \frac{1}{2}\sum_{ars}\frac{v_{rsia}v_{jars}}{\omega_n + \epsilon_a - \epsilon_r - \epsilon_s} + \\ + \frac{1}{2}\sum_{abr}\frac{v_{abir}v_{jrab}}{\omega_n + \epsilon_r - \epsilon_a - \epsilon_b}, \tag{4.14}$$

where v_{ijkl} are the antisymmetrized two-body integrals in the molecular orbital (MO) basis in the chemist's notation. The occupied orbitals are labeled a, b and unoccupied orbitals are labeled r, s; the i and j labels can refer to any orbital. The frequencies ($\omega_n = \omega_n^{'} + i\eta$) are constructed as a *real* axis $\omega_n^{'}$ grid with a small imaginary broadening term $i\eta = 0.001i$. The self-energy is computed in the MO basis on the real axis, in contrast to the imaginary axis, where it was computed in the AO basis. We would like to emphasize that we do not obtain the self-energy on the real axis through an iterative GF2 procedure, instead we perform a "single shot" self-energy evaluation which is constructed using the Fock matrix that was obtained in the self-consistent GF2 procedure.

Once the real axis second-order self-energy is evaluated, we are able to find the roots of Dyson's equation, where we ignore the off-diagonal elements of $\mathbf{\Sigma}^{(2)(\omega_n)}$ and solve only

$$\prod_i (\omega_n - \epsilon_i - \Sigma^{(2)}_{ii}(\omega_n)) = 0. \tag{4.15}$$

This expression gives the lowest-order correction to the Koopmans' theorem IP. Then the corrected IPs are expressed as

$$\epsilon_i' = \epsilon_i + \Sigma_{ii}(\epsilon_i) \tag{4.16}$$

where ϵ_i' is the corrected IP. We refer to the IP/EA obtained in this manner as HF+$\Sigma^{(2)}_{ii}$. We can

evaluate Eq. 4.16 iteratively by reevaluating the self-energy at the new value ϵ_i' until convergence is reached. Due to the iterative nature it is not always easy or even possible to converge Eq 4.16. To help with convergence, we introduce a simple damping scheme

$$\Sigma_{ii}^{(2)\prime\prime} = \alpha\Sigma_{ii}^{(2)} + (1-\alpha)\Sigma_{ii}^{(2)\prime} \tag{4.17}$$

where α is a damping parameter between 0.0 and 1.0, $\Sigma_{ii}^{(2)}$ is the self-energy from the previous iteration, and $\Sigma_{ii}^{(2)\prime}$ is the updated self-energy. We refer to the IP/EA obtained in this manner as HF+iter $\Sigma_{ii}^{(2)}$.

4.3.3 F(GF2)+$\Sigma^{(2)}$

In the F(GF2)+$\Sigma^{(2)}$ approach the the self-energy is built on the real axis according to the Eq. **??**, however, here the eigenvalues of the Fock matrix present in the denominators are obtained from the diagonalization of the Fock matrix that comes from the fully converged GF2 procedure on the imaginary axis. Such a Fock matrix depends on the correlated one-body density matrix through the correlated Green's function, as described in Sec. 4.2. For low temperatures, for predominantly single reference cases, the occupied orbitals still have occupancies arround 2, while the unoccupied orbitals have occupancies near 0. Using such a full self-energy matrix on the real axis, the Green's function is built according to the Dyson equation

$$\mathbf{G}(\omega_n) = [(\omega_n + \mu)\mathbf{1} - \epsilon - \mathbf{\Sigma}^{(2)}(\omega_n)]^{-1} \tag{4.18}$$

where ϵ is the matrix of eigenvalues coming from the diagonalization of the converged Fock matrix from GF2, μ is the chemical potential, and the ω_n grid is the same as described in the previous section. We would like to emphasize once again that we do not iterate $G(\omega_n)$ on the real axis. Note that in contrast to the HF+$\Sigma_{ii}^{(2)}$ and HF+iter $\Sigma_{ii}^{(2)}$ the F(GF2)+$\Sigma^{(2)}$ approach includes all off-diagonal elements of $\mathbf{\Sigma}^{(2)}$.

Using the real axis Green's function, we evaluate the spectral function as

$$A(\omega_n) = \frac{-1}{\pi}\mathrm{Tr}[\mathrm{Im}\mathbf{G}(\omega_\mathrm{n})] \tag{4.19}$$

with peaks corresponding to the IPs/EAs. We have chosen to call this method of spectra evaluation as F(GF2)+$\Sigma^{(2)}$, referring to the fact that the Fock matrix **F** comes from the converged GF2 calculation on the imaginary axis.

4.4 Results

We have benchmarked these methods for closed shell atoms using Dunning's augmented correlation consistent basis sets (aug-cc-pVXZ, X=D,T,Q). We compare against UCCSD(T) energy differences and experimental values when available. Additionally, we have computed the ionization potentials of several molecules in the basis aug-cc-pVDZ and for DNA bases (adenine, thymine, cytosine) and the RNA base uracil in Dunning's cc-pVDZ basis.

4.4.1 Ionization Potentials

The results for atoms can be found in Fig. 4.1. For these cases, UCCSD(T) energy differences reproduce the experimental IPs very accurately. As expected, the Koopman's theorem IPs from Hartree-Fock overestimate the experimental IPs. All of the Green's function methods tend to underestimate the IPs for these systems. The Extended Koopmans' theorem IPs underestimate the most, sometimes giving worse or similar agreement to Koopmans' theorem. For these systems the method that most closely recovers the IPs is HF+$\Sigma^{(2)}_{ii}$, but this is most likely fortuitous. While both iterated methods have lowered IPs in comparison with non-iterated ones, they are in principle independent of the reference.

The results for molecules are given in Table 4.1. It is clear from these results that the HF + $\Sigma^{(2)}_{\mathrm{ii}}$ method behaves erratically, sometimes giving a good result and sometimes giving a result which differs by several electron volts in comparison with the experimental value. This indicates that

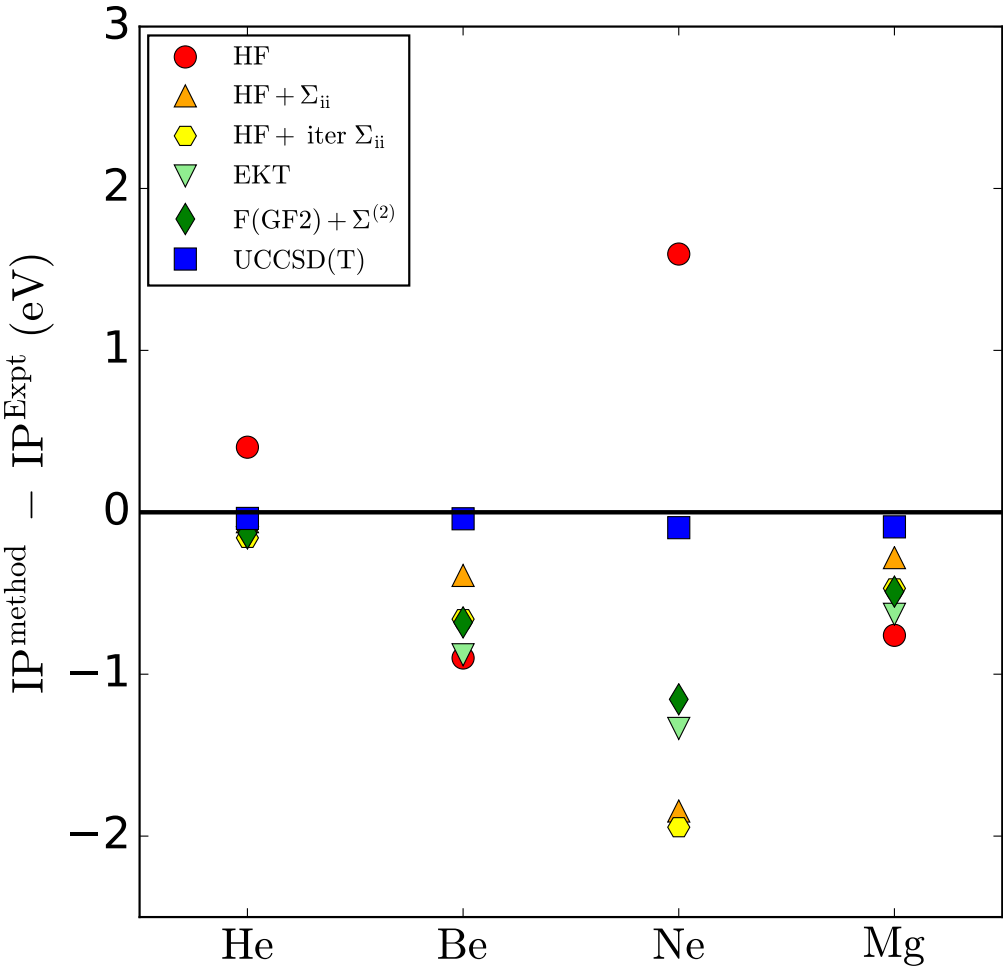

Figure 4.1: Ionization potentials for atoms calculated with basis aug-cc-pVTZ. Shown here are differences from experimental values. Units in eV.

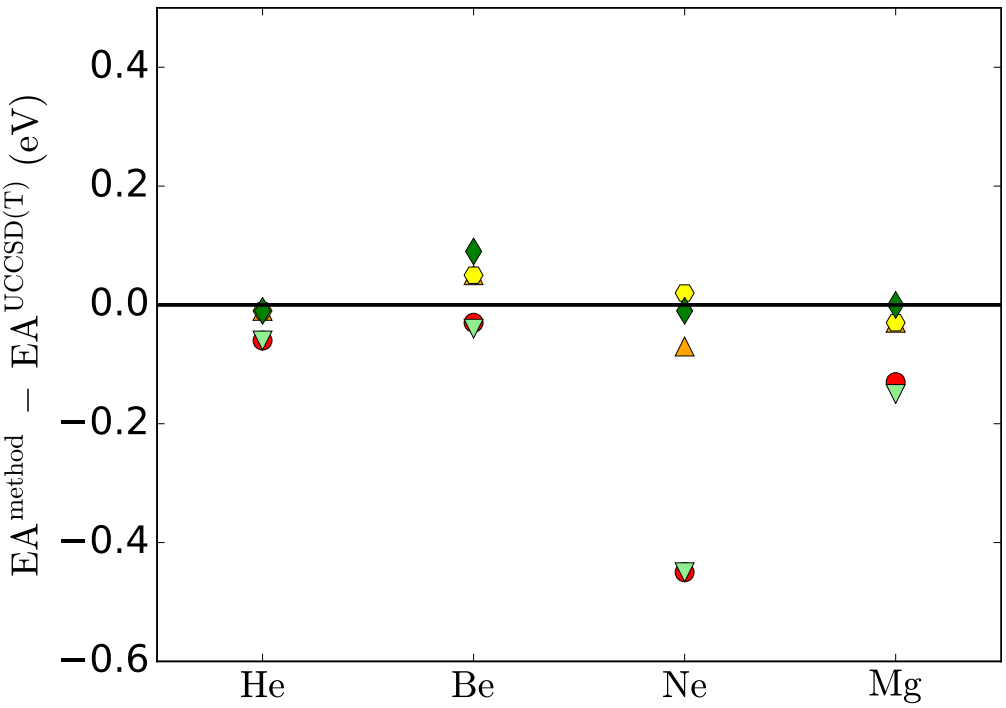

Figure 4.2: Electron affinities for atoms calculated with basis aug-cc-pVTZ. Shown here are differences from UCCSD(T) calculations in the same basis. Units in eV.

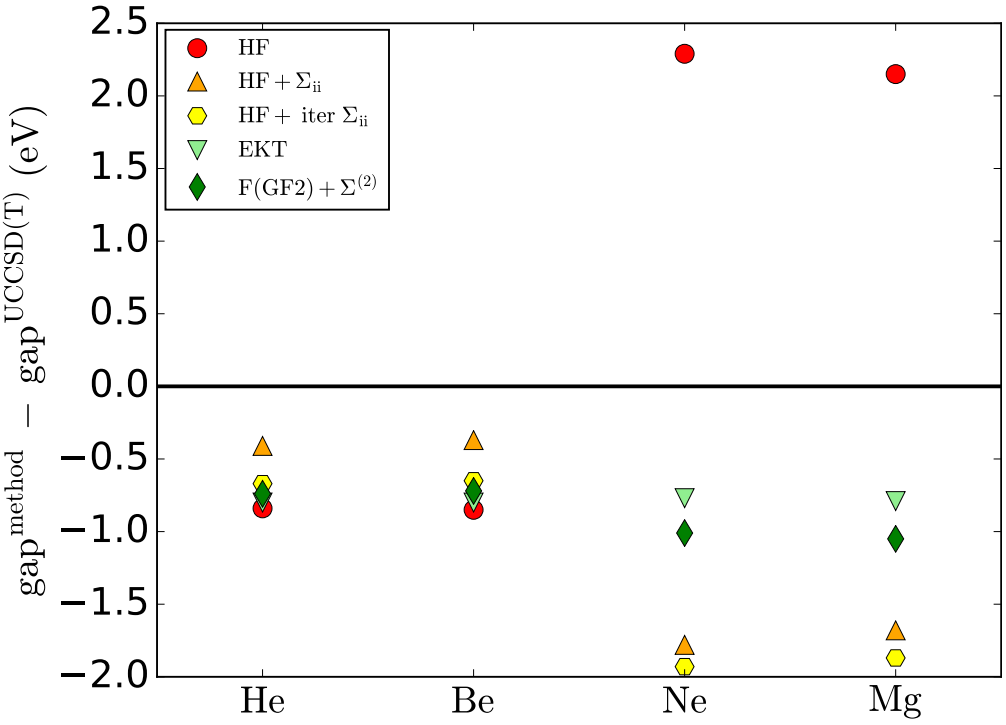

Figure 4.3: Fundamental gaps for atoms calculated with basis aug-cc-pVTZ. Shown here are differences from UCCSD(T) calculations in the same basis. Units in eV.

	F(GF2) + $\Sigma^{(2)}$	EKT	HF	HF+$\Sigma^{(2)}_{ii}$	HF + iter $\Sigma^{(2)}_{ii}$	UCCSD(T)	GW[92]	Expt
Be_2	6.51	6.21	6.62	6.99	6.55	7.42		
BH_3	12.93	12.82	13.52	13.04	12.87	13.17	12.79- 13.28	12.03
C_2H_2 (acetylene)	10.79	10.24	11.19	11.13	10.68	11.36	10.93-11.35	11.49
C_2H_4 (ethylene)	9.85	9.54	10.21	10.1	9.75	10.55	10.17-10.68	10.51
CO	13.22	12.2	15.09	13.8	12.87	13.8	13.37-14.33	14.01
CO_2	12.56	11.71	14.82	12.48	-	13.61	13.04-13.81	13.78
H_2CO (formaldehyde)	9.62	9.12	12.02	9.54	9.01	10.74	10.32-11.02	10.88
H_2O	11.48	11.31	13.86	10.91	10.57	12.54	11.92-12.75	12.65
H_2O_2	10.18	9.51	13.31	9.53	-	11.46	10.92-11.58	11.70
HCN	13.13	12.26	13.5	13.43	-	13.62	13.13-13.87	13.61
HF	14.86	14.68	17.68	13.91	13.71	16.02	15.26-16.24	16.12
Li_2	4.98	4.69	4.95	5.17	5.01	5.23	4.99-5.43	4.73
LiF	10.3	9.89	12.91	8.85	8.36	11.37	9.95-11.84	11.30
LiH	7.82	7.77	8.2	7.89	7.77	7.94	6.54-7.85	7.90
MgH_2	9.70	9.80	10.09	9.81	9.67	9.76		
N_2	14.29	13.53	17.26	14.52	13.71	15.36	14.72-15.43	15.58
Na_2	4.61	4.67	4.51	4.77	4.64	4.85	4.83-5.03	4.89
NaF	8.51	8.38	11.59	4.97	6.36	9.98		
NaH	6.83	6.82	7.43	6.84	6.83	7.04		
NaLi	4.77	4.69	4.71	4.95	4.8	5.01		
NaOH	6.82	6.42	9.11	5.59	-	7.86		
NH_3	9.94	9.86	11.67	9.79	9.46	10.76	10.27-10.93	10.82

Table 4.1: Ionization potentials in eV for closed shell molecules calculated with aug-cc-pVDZ.

as the system size becomes larger this method may not be reliable, and also hints that the results obtained for the atoms are a result of a fortunate cancellation of error, and not due to the accuracy of the method.

There is no method for IP presented here that is able to consistently give an IP that is close to experiment aside from UCCSD(T), which is a very expensive method in comparison with the other methods. Due to the scaling, it would be challenging to use this method for very large systems. We can see from the Green's function methods that even at the same level of theory (second-order in this case) the approximation chosen to evaluate the IP can have a drastic effect on the value obtained. Therefore, one must exercise caution when choosing a method of evaluation and trying to make meaningful comparisons between IPs obtained using different methods.

4.4.2 Electron Affinities

Electron affinities for some atoms can be found in Fig. 4.2. We compare our results with EAs calculated from energy differences between UCCSD(T) neutral and charged species due to lack of available experimental data for this property. The HF and EKT values are quite similar and are in general quite far from the UCCSD(T) reference. The F(GF2) + $\Sigma^{(2)}$ method gives consistent and accurate EAs in comparison with UCCSD(T). Similar to the IPs, the EAs with the HF+$\Sigma^{(2)}_{ii}$ method give good results for atoms, but this is once again most likely fortuitous. Iteration using the HF+iter $\Sigma^{(2)}_{ii}$ method can sometimes improve the accuracy, but this is unpredictable. We would like to emphasize that this iteration is only for the diagonal elements of the self-energy, and since we are only updating the self-energy, this method is still dependent on the HF reference.

Electron affinities for the molecules can be found in Table 4.2. It is clear that HF and EKT give results that underestimate UCCSD(T) values in general. When the UCCSD(T) EA is positive, both of these methods often fail qualitatively and give a negative EA. The HF + $\Sigma^{(2)}_{ii}$ method is typically a good correction to HF, but this is highly dependent on the fact that HF gives a good value. Iteration in the HF + iter$\Sigma^{(2)}_{ii}$ method does not necessarily bring the EA into better agreement with UCCSD(T). F(GF2) + $\Sigma^{(2)}$ consistently gives EAs that agree well with UCCSD(T) across all systems.

Comparing the smaller molecules to larger ones indicates that HF and EKT are less accurate as the system size grows. Therefore, methods that depend on the starting reference may tend to become less accurate as the system size increases. For this reason, fully iterated methods are advantageous.

4.4.3 Fundamental Gap

For all atoms and molecules, the accuracy of the fundamental gap (gap = IP-EA) is heavily dependent on the accuracy of the EA, as all methods gave relatively similar results for the IP, but can give drastically different values for EA. F(GF2) + $\Sigma^{(2)}$ performs very well for this reason, both in

	F(GF2) + $\Sigma^{(2)}$	EKT	HF	HF+$\Sigma^{(2)}_{ii}$	HF + iter $\Sigma^{(2)}_{ii}$	UCCSD(T)
Be_2	0.44	-0.30	-0.21	0.39	0.52	0.34
BH_3	-0.15	-0.92	-0.88	-0.35	-0.31	-0.15
C_2H_2 (acetylene)	-0.97	-1.09	-1.08	-0.97	-0.97	-0.99
C_2H_4 (ethylene)	-1.20	-1.37	-1.37	-1.22	-1.20	-1.22
CO	-1.75	-2.34	-2.15	-1.83	-1.78	-1.81
CO_2	-2.22	-2.38	-2.34	-2.21	-	-2.23
H_2CO (formaldehyde)	-0.92	-1.42	-1.38	-0.74	-1.33	-1.19
H_2O	-0.74	-0.93	-0.96	-0.79	-0.74	-0.75
H_2O_2	-1.04	-1.37	-1.38	-1.18	-	-1.16
HCN	-0.67	-0.83	-0.79	-0.64	-	-0.69
HF	-0.80	-0.95	-0.97	-0.83	-0.80	-0.80
Li_2	0.23	-0.10	-0.08	0.16	0.17	0.32
LiF	0.32	0.27	0.29	0.33	0.32	0.34
LiH	0.27	0.20	0.21	0.27	0.27	0.30
MgH_2	-0.56	-0.65	-0.65	-0.57	-0.35	-0.50
N_2	-2.61	-2.81	-3.39	-3.18	-2.60	-2.60
Na_2	0.32	-0.05	-0.01	0.28	0.29	0.36
NaF	0.40	0.43	0.44	0.27	0.47	0.48
NaH	0.29	0.22	0.24	0.30	0.30	0.32
NaLi	0.30	-0.07	-0.04	0.25	0.25	0.35
NaOH	0.38	0.32	0.31	0.36	-	0.39
NH_3	-0.74	-0.94	-0.98	-0.79	-0.75	-0.75

Table 4.2: Electron affinities in eV for closed shell molecules calculated with aug-cc-pVDZ.

consistency across different systems and in overall accuracy. The fundamental gaps for atoms can be found in Fig. 4.3.

The fundamental gaps for molecules can be found in Table When HF + $\Sigma_{ii}^{(2)}$ gives a reasonable EA, the value for fundamental gap is often good as well. For many systems EKT is able to give agreement comparable to other Green's function methods, but this is due to some fortunate error cancellation between IP and EA. This was not the case for the DNA bases, which were much larger.

4.4.4 DNA and RNA nucleobases

In this section, we apply our GF2 method to DNA bases adenine, thymine, and cytosine and the RNA base uracil. Due to their obvious biological importance, there is a wealth of experimental and theoretical data regarding their electronic properties. As these bases exist in several tautomeric forms that are close in energy, it is often necessary to use a combination of experiment and accurate theories to resolve their spectra[93]. We present the IPs and EAs of these molecules using GF2 and our various procedures to extract these quantities.

We have computed IPs for these nucleobases, and these results can be found in Fig. 4.4. In general, no method is able to recover the IP with great accuracy, but these data allow us to understand some trends regarding how the methods behave. As expected, HF tends to overestimate in comparison with experiment, and using the diagonal approximation HF + $\Sigma_{ii}^{(2)}$ lowers the value of IP, but does not always give a more accurate answer, especially if the HF IP is already quite close to the experimental IP. EKT underestimates IP for these systems, as does F(GF2) + $\Sigma_{ii}^{(2)}$, but these two methods are reference independent, whereas HF + $\Sigma_{ii}^{(2)}$ relies on the HF value giving a reasonable guess for the IP.

Also shown in Fig. 4.4 are the EAs. HF underestimates the EA by several electron volts in all cases. Including the diagonal correction through the HF + $\Sigma_{ii}^{(2)}$ vastly improves the agreement with experiment for all of these systems. The inclusion of correlation through EKT gives worse agreement than HF, lowering the EA by over 1 eV in all cases. The F(GF2) + $\Sigma^{(2)}$ method consistently gives good agreement in comparison with the other methods presented here.

	F(GF2) + $\Sigma^{(2)}$	EKT	HF	HF+$\Sigma^{(2)}_{ii}$	HF + iter $\Sigma^{(2)}_{ii}$	UCCSD(T)
Be_2	6.07	6.51	6.83	6.60	6.03	7.09
BH_3	13.08	13.75	14.41	13.39	13.18	13.32
C_2H_2 (acetylene)	11.75	11.33	12.27	12.10	11.65	12.34
C_2H_4 (ethylene)	11.06	10.90	11.58	11.32	10.95	11.77
CO	14.97	14.55	17.24	15.63	14.64	15.61
CO_2	14.78	14.08	17.16	14.69	-	15.84
H_2CO (formaldehyde)	10.54	10.54	13.40	10.28	10.34	11.93
H_2O	12.23	12.24	14.83	11.70	11.31	13.29
H_2O_2	11.22	10.88	14.68	10.71	-	12.63
HCN	13.80	13.09	14.28	14.07	-	14.31
HF	15.66	15.62	18.64	14.75	14.51	16.82
Li_2	4.75	4.80	5.03	5.00	4.84	4.91
LiF	9.99	9.62	12.62	8.52	8.03	11.03
LiH	7.54	7.56	7.99	7.62	7.49	7.64
MgH_2	10.26	10.45	10.73	10.38	10.02	10.26
N_2	16.91	16.33	20.65	17.69	16.31	17.96
Na_2	4.29	4.73	4.52	4.48	4.34	4.49
NaF	8.10	7.95	11.15	4.70	5.90	9.50
NaH	6.54	6.60	7.19	6.54	6.53	6.72
NaLi	4.48	4.77	4.74	4.70	4.55	4.65
NaOH	6.44	6.10	8.80	5.24	-	7.47
NH_3	10.68	10.80	12.65	10.58	10.20	11.51

Table 4.3: Fundamental gaps in eV for closed shell molecules calculated with aug-cc-pVDZ.

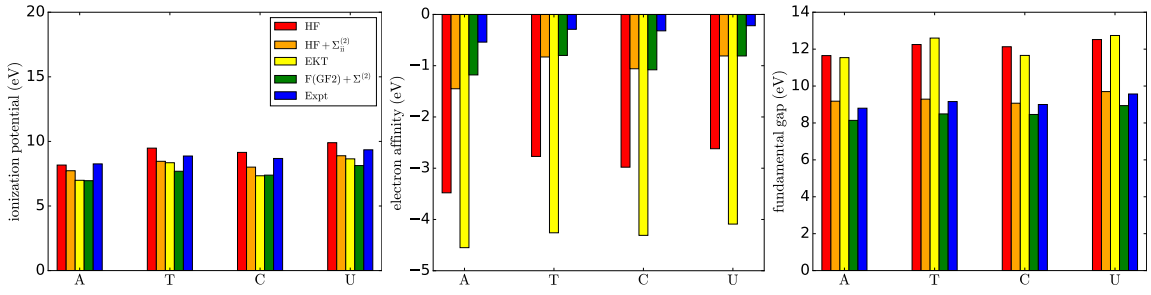

Figure 4.4: Ionization potentials, electron affinities, and fundamental gap for DNA/RNA bases (A=Adenine, T=Thymine, C=Cytosine, U=Uracil). Basis cc-pVDZ. Geometries taken from Ref. [94].

As with the atoms and small molecules in the earlier section, the agreement of the fundamental gap with experiment is almost entirely dependent upon the agreement of the EA with experiment. The DNA/RNA bases illustrate this point clearly. In all cases, GF2 gives the closest gap to experiment, due largely to the acceptable accuracy of the IP and the comparitively good accuracy of the EA. Because EKT drastically underestimates the EA, the gaps from EKT for these systems are several electron volts higher than the experimental gaps, and more closely resemble the Hartree-Fock gaps. The method HF + $\Sigma_{ii}^{(2)}$ also gives good agreement with the gap for these systems.

4.5 Singlet-Triplet Gap Evaluation

We investigated the ability of our GF2 method to approximate singlet-triplet gaps. We do so by evaluating the energy difference between the singlet and triplet state, which requires an unrestricted formalism. We highlight the differences between the restricted and unrestricted GF2 algorithms here. The geometries were obtained from Ref. [94].

To accommodate unpaired electrons, we require two density matrices, $\mathbf{P}^{\alpha}$ and $\mathbf{P}^{\beta}$, for alpha spin and beta spin, as well as their respective Fock matrices, $\mathbf{F}^{\alpha}$ and $\mathbf{F}^{\beta}$. Using these quantities, we can build the Green's functions iteratively using Eqns. 4.1 - 4.3 given in Sec. 4.2. We now require two bisections to find the chemical potentials μ^{α} and μ^{β}.

We have calculated singlet-triplet gaps for some molecular systems. These data can be found

	GF2	MP2	UCCSD	UCCSD(T)	Expt
ethene	4.63	4.58	4.41	4.53	4.36-4.6
benzene	4.77	5.81	5.42	5.40	3.66
butadiene	3.47	3.53	3.38	3.41	3.22
naphthalene	2.02	3.90	3.28	3.26	2.64
cyclopentadiene	3.44	3.50	3.27	3.32	4.7

Table 4.4: Singlet Triplet Gaps in eV. Basis cc-pVDZ. Experimental gaps from Ref. [95].

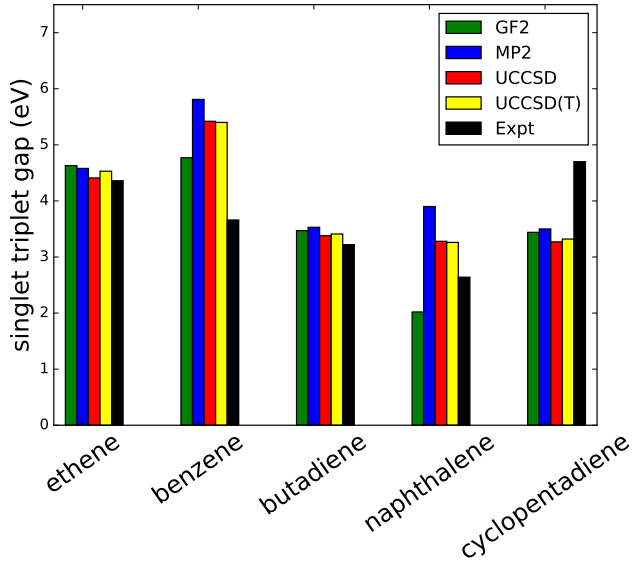

Figure 4.5: Singlet-triplet gaps aug-cc-pVDZ evaluated with unrestricted GF2.

in Table 4.4. We have compared our results with MP2, CCSD, and CCSD(T) results. We are able to obtain reasonable agreement with experimental gaps for these systems. For smaller systems, GF2 shows more agreement with MP2, while for larger systems the GF2 result can differ by over 1 eV. It is worth noting that these systems are calculated in the cc-pVDZ basis, which is a rather modest basis.

4.6 Conclusions

The goal of this work was to investigate the ability of a temperature-dependent Green's function method to obtain IPs and EAs for nontrivial chemical systems. To this end, we calculated several atoms, small molecules, and slightly larger molecules, and explored a variety of ways to extract real axis data from the imaginary axis Green's function. The simplest way we attempted to carry this out was using EKT to obtain IPs and EAs directly from the imaginary axis. We found in general that this was an unreliable approach and can give IPs and especially EAs that are very far from experimental values or UCCSD(T) values, which are thought to be highly accurate. To explore another route, we relied on the fact that the converged density matrix is the same on both the real and imaginary axis. From this density, we are able to construct a new Fock matrix, and then build a Green's function on the real frequency axis. There are different approximations to employ in order to evaluate the self-energy, including a diagonal approximation (HF+$\Sigma_{\mathrm{i}}^{(2)}$i), an interated diagonal approximation (HF+iter Sigma$_{\mathrm{i}}^{(2)}$i, and a full construction of the self-energy (F+$\Sigma_{ii}^{(2)}$).

In this work we have investigated the ability of GF2 to calculate IPs, EAs, fundamental gaps, and singlet-triplet gaps for a range of atomic and molecular systems. In general, it was very difficult to obtain EAs in good agreement with UCCSD(T) using any method. There was no method that emerged as the superior method, and results could vary based on the type of system. The most consistent method was building the full self-energy on the real axis, including all of the diagonal elements. This method (F+$\Sigma_{ii}^{(2)}$) was able to give the results similar in accuracy across a range of systems. Although all quantities computed with the Green's function in this work were done with a second-order evaluation of the self-energy, different evaluation methods can give values for these quantities that differ by several electron volts from each other.

For smaller systems such as atoms or molecules, there is some indication that a method gives good agreement with experiment due to error cancellation rather than due to accuracy of the method. Fully self-consistent Green's function methods give consistent results across all systems considered in this work, while methods such as EKT can benefit from error cancellations or can

fail drastically. For the DNA bases we found that the IPs were recovered reasonably by all of the methods considered, while EAs for these systems showed great deviations between the methods. Overall, it is unclear whether including more correlation leads to more reliable accuracy for these methods, and further study would be needed to uncover the reasons for the numerical or physical reasons for the deviations of each method. In general, we have demonstrated that it is non-trivial to obtain spectra from the imaginary axis, and that severe caution is needed when evaluating spectra from different methods and approximations.

4.6.1 Supplemental Information

aug-cc-pVDZ

	F(GF2) + $\Sigma^{(2)}$	EKT	HF	HF+$\Sigma^{(2)}_{ii}$	HF + iter $\Sigma^{(2)}_{ii}$	UCCSD(T)	Expt
He	24.32	24.26	24.96	24.34	24.28	24.36	24.578
Be	8.59	8.38	8.42	8.86	8.62	9.29	9.32
Ne	20.41	20.32	23.21	19.49	19.52	21.42	21.565
Mg	7.09	6.96	6.89	7.29	7.12	7.53	7.65

aug-cc-pVTZ

	F(GF2) + $\Sigma^{(2)}$	EKT	HF	HF+$\Sigma^{(2)}_{ii}$	HF + iter $\Sigma^{(2)}_{ii}$	UCCSD(T)	Expt
He	24.45	24.42	24.98	24.52	24.42	24.54	24.578
Be	8.64	8.44	8.42	8.93	8.66	9.28	9.32
Ne	20.41	20.23	23.16	19.72	19.62	21.47	21.565
Mg	7.16	7.02	6.89	7.37	7.18	7.56	7.65

aug-cc-pVQZ

	F(GF2) + $\Sigma^{(2)}$	EKT	HF	HF+$\Sigma^{(2)}_{ii}$	HF + iter $\Sigma^{(2)}_{ii}$	UCCSD(T)	Expt
He	24.49	24.47	24.98	24.57	24.46	24.56	24.578
Be	8.66	8.46	8.42	8.97	8.69	9.30	9.32
Ne	20.46	20.24	23.15	19.87	-	21.55	21.565
Mg	7.19	7.08	6.89	7.42	7.21	7.58	7.65

Table 4.5: Ionization potentials in eV for atoms calculated in aug-cc-pVXZ (X=D,Z,Q) using different methods. A dash indicates no convergence.

aug-cc-pVDZ

	F(GF2) + $\Sigma^{(2)}$	EKT	HF	HF+$\Sigma^{(2)}_{ii}$	HF + iter $\Sigma^{(2)}_{ii}$	UCCSD(T)
He	-4.68	-4.75	-4.74	-4.68	-4.68	-4.67
Be	-0.33	-0.47	-0.45	-0.36	-0.36	-0.39
Ne	-7.32	-7.65	-7.82	-7.47	-7.29	-7.32
Mg	-0.30	-0.48	-0.45	-0.32	-0.32	-0.26

aug-cc-pVTZ

	F(GF2) + $\Sigma^{(2)}$	EKT	HF	HF+$\Sigma^{(2)}_{ii}$	HF + iter $\Sigma^{(2)}_{ii}$	UCCSD(T)
He	-2.96	-3.01	-3.01	-2.96	-2.96	-2.95
Be	-0.28	-0.41	-0.40	-0.32	-0.32	-0.37
Ne	-6.11	-6.55	-6.55	-6.17	-6.08	-6.10
Mg	-0.25	-0.40	-0.38	-0.28	-0.28	-0.25

aug-cc-pVQZ

	F(GF2) + $\Sigma^{(2)}$	EKT	HF	HF+$\Sigma^{(2)}_{ii}$	HF + iter $\Sigma^{(2)}_{ii}$	UCCSD(T)
He	-2.63	-2.69	-2.69	-2.64	-2.64	-2.63
Be	-0.26	-0.38	-0.37	-0.30	-0.31	-0.34
Ne	-5.49	-5.62	-5.62	-5.52	-	-5.29
Mg	-0.23	-0.38	-0.36	-0.27	-0.27	-0.22

Table 4.6: Electron affinities in eV for atoms caclulated in aug-cc-pVXZ (X=D,Z,Q) using different methods. A dash indicates no convergence.

CHAPTER 5

Temperature-Dependent Configuration Interaction Impurity Solver for Quantum Embedding

Recently, in the quantum chemistry community, more attention has been given to quantum embedding methods. In particular, rigorous quantum embedding theories that have non-trivial electron exchange between the impurity and the environment have seen much development in recent years. Such methods include density matrix embedding theory (DMET), Green's function embedding, and density functional (DFT) embedding. An excellent review, discussing the relationship of these techniques, is given in [96].

In previous work, a zero-temperature RASCI solver was shown to give good agreement with exact diagonalization results, but was able to treat much larger active spaces than methods such as exact diagonalization (ED). [97] However, to the best of our knowledge, no such RASCI solver exists that includes the effects of temperature. Including temperature dependence in an impurity with realistic interactions is nontrivial. In this work, we aim to include the effects of temperature by building an ensemble Green's function, including all of the appreciably occupied low lying excited states in the Green's function. This will allow calculation of larger systems than the ones accessible by ED and additionally will not suffer from the sign problem that plagues CTQMC methods at low temperatures. Additionally, the solver is able to treat general interactions at polynomial cost and will be useful in embedding schemes such as dynamical mean field theory (DMFT) and self-energy embedding theory (SEET).

5.1 Restricted Configuration Interaction (RASCI) Method

The configuration interaction (CI) method is a post Hartree-Fock wavefunction method that is widely known in the quantum chemistry community. In theory, this method can provide the exact energies of the ground state as well as the excited states of a system. This is achieved by diagonalizing the N-electron Hamiltonian in the basis of N-electron Slater determinants, or representing the wavefunction as a linear combination of these Slater determinants and minimizing the energy.

The CI wavefunction has the form

$$|\Phi_0\rangle = c_0 |\Psi_0\rangle + \sum_{ar} c_a^r |\Psi_a^r\rangle + \left(\frac{1}{2!}\right)^2 \sum_{abrs} c_{ab}^{rs} |\Psi_{ab}^{rs}\rangle + \left(\frac{1}{3!}\right)^2 \sum_{abcrst} c_{abc}^{rst} |\Psi_{abc}^{rst}\rangle + \cdots \tag{5.1}$$

where a,b,c... refer to occupied orbitals and r,s,t... refer to virtual orbitals. While this method is simple in principle, it is computationally very demanding and can only be carried out for small systems (about 12 basis functions).

The number of possible Slater determinants is given as $\binom{2k}{N}$ for 2k spin orbitals and N electrons. This number grows prohibitively large for even small systems. In practice, the wavefunction is often truncated to only include excitations up to a certain extent, such as configuration interaction singles doubles (CISD), singles doubles triples (CISDT), etc. A pedagogical introduction to the CI method can be found in Ref. [98].

5.2 Impurity Models

Quantum embedding can be generally understood as the partitioning of a larger system into regions - an active region or “impurity” and an environment region or “bath” - to reduce the computational cost of studying electron correlations. The impurity region is treated with a higher-level, more accurate calculation, while the environment is treated non-trivially with a more affordable calculation. Such embedding schemes have been used in condensed matter[99], quantum chemistry[100], and materials science [101].

The impurity problem maps correlated electron problems, which are challenging or sometimes prohibitively expensive to solve, to auxiliary models that include few explicit interactions coupled to a bath of electrons. This description can significantly reduce the calculation cost and make solving the problem numerically tractable.

In its general form, a quantum impurity model is defined by the Hamiltonian

$$H = H_{loc} + H_{bath} + H_{hyb}, \tag{5.2}$$

$$H_{loc} = \sum_{pq} t_{pq} d_p^\dagger d_q + \sum_{pqrs} I_{pqrs} d_p^\dagger d_q^\dagger d_r d_s, \tag{5.3}$$

$$H_{bath} = \sum_k \epsilon_k c_k^\dagger c_k, \tag{5.4}$$

$$H_{hyb} = \sum_{kp} V_{kp} c_k^\dagger d_p + h.c., \tag{5.5}$$

where H_{loc} contains the parent impurity orbitals. In most of the embedding theories designed to treat realistic systems, both the one- and two-body integrals, here t_{pq} and I_{pqrs}, respectively, are completely general and no simplifying structure of either t_{pq} or I_{pqrs} can be assumed. The bath Hamiltonian can always be expressed in a diagonal form, as presented in Eq. 5.4. The bath and impurity interaction is described by H_{hyb} and the interactions are described by coupling terms V_{kp} from Eq. 5.5.

5.3 Finite temperature Lanczos

5.3.1 Matsubara Green's Function from Lanczos procedure

The finite temperature Green's function can be expressed as

$$G_{pq}(i\omega) = \frac{1}{Z} \sum_m e^{-\beta E_m^{(N)}} G_{pq}^{(m)}(i\omega) \tag{5.6}$$

where $Z = \sum_n e^{-\beta E_n^{(N)}}$ is the partition function and $G_{pq}^{(m)}$ is given as

$$G_{pq}^{(m)}(i\omega) = \langle \Psi_m | c_p^\dagger \frac{1}{i\omega + (H - E_m)} c_q | \Psi_m \rangle + \langle \Psi_m | c_p \frac{1}{i\omega - (H - E_m)} c_q^\dagger | \Psi_m \rangle \tag{5.7}$$

where E_m and Ψ_m are the energy and wavefunction of state m, $c_{p/q}$ and $c_{p/q}^\dagger$ are the annihilation and creation operators for p and q spins. The frequencies $i\omega$ are the imaginary Matsubara frequencies given as $i\omega = \frac{(2n+1)i\pi}{\beta}$ for n = 0, 1, 2..., and $\beta = \frac{1}{kT}$ is the inverse temperature.

For low temperatures, only a few of the lowest states will have an appreciably large Boltzmann factor. These few lowest states can be used as an approximation to the exact Green's function. In order to avoid an expensive diagonalization of the Hamiltonian, a Lanczos procedure can be used to find the few lowest eigenvalues. The procedure begin with a Davidson algorithm to diagonalize the CI Hamiltonian and obtain the energies E_m and the vectors $|\Psi_m\rangle$. The energies below a cutoff energy E_{cutoff} and their corresponding vectors are chosen and acted on with the operators $c_{p/q}$ and $c_{p/q}^\dagger$. These vectors $c_{p/q}|\Psi_m\rangle$ and $c_{p/q}^\dagger|\Psi_m\rangle$ are the starting vectors of the Lanczos procedure, which are normalized and from here denoted as $|\phi_0\rangle$. A sequence of mutually orthogonal vectors is created from the recursion relation

$$|\phi_{n+1}\rangle = H|\phi_0\rangle - a_n|\phi_n\rangle - b_n^2|\phi_{n-1}\rangle \tag{5.8}$$

where

$$\begin{aligned} a_n &= \frac{\langle \phi_n | H | \phi_n \rangle}{\langle \phi_0 | \phi_0 \rangle} \\ b_n^2 &= \frac{\langle \phi_n | \phi_n \rangle}{\langle \phi_{n-1} | \phi_{n-1} \rangle} \\ b_0 &= 0 \end{aligned} \tag{5.9}$$

The Lanczos procedure returns a tridiagonal matrix T_N

$$T_N = \begin{bmatrix} a_0 & b_1 & & 0 \\ b_1 & \ddots & \ddots & \\ & \ddots & \ddots & b_N \\ 0 & & b_N & a_N \end{bmatrix} \tag{5.10}$$

in the projected Krylov subspace $\mathcal{K} = \text{span}\left\{|\phi_0\rangle, H|\phi_0\rangle, H^2|\phi_0\rangle, \cdots, H^M|\phi_0\rangle\right\}$.

The Green's function can then be constructed as

$$G_{pp}(i\omega) = \frac{n_p}{i\omega - E_m + a_0 - \frac{b_1^2}{i\omega - E_m + a_1 - \ldots}} + \frac{1 - n_p}{i\omega + E_m + a_0 - \frac{b_1^2}{i\omega + E_m + a_1 - \ldots}} \tag{5.11}$$

where $n_p = \langle \Psi_m | c_p^\dagger c_p | \Psi_m \rangle$. The off-diagonal elements can be constructed using the following set of relationships

$$G^+_{pq}(i\omega) = \langle \Psi_m | (c_p + c_q) \frac{1}{\omega - H + E_m} (c_p + c_q)^\dagger | \Psi_m \rangle \tag{5.12}$$

$$G_{pq}(i\omega) = G_{qp}(i\omega) \tag{5.13}$$

$$G_{pq}(i\omega) = \frac{1}{2}(G^+_{pq}(i\omega) - G_{pp}(i\omega) - G_{qq}(i\omega)) \tag{5.14}$$

The quantity G^+_{pq} from Eq. 5.12 can be calculated using the continued fraction expression in Eq. 5.11. This procedure is a memory efficient way to obtain the lowest eigenvalues of the matrix, without resorting to expensive exact diagonalization procedures.

This procedure is carried out for each E_m and Ψ_m included below the E_{cutoff}. The final ensemble Green's function is constructed using Eq. 5.6. In general, one can consider this procedure a mapping of a CI wavefunction to a temperature dependent Green's function.

5.4 Results

5.4.1 Hubbard Impurity Models

The Hubbard model is a simple model of interacting particles on a lattice with on-site interactions. This model is capable of describing the transition between conductors and insulators. The Hamiltonian for the Hubbard impurity model, including the impurity orbitals and the bath is given as

$$H = U\Big(n_\uparrow n_\downarrow - \frac{n_\uparrow + n_\downarrow}{2}\Big) + \sum_{i\sigma} c^\dagger_{i\sigma} c_{i\sigma} + \sum_{i\sigma} V_i c^\dagger_{i\sigma} d_\sigma + h.c. \tag{5.15}$$

where U describes the potential energy of the onsite electrons, and the annihilation and creation operators $d^{(\dagger)}$ and $c^{(\dagger)}$, destroy and create electrons in the impurity and bath, respectively. In the next two sections, I present the results of the study of the 1D and 2D Hubbard impurity with the RASCI solver, including temperature effects. All calculations were carried out in the natural orbital basis.

5.4.2 Results for 1D Hubbard Impurity Model

The RAS-CI solver was used to calculate a one-dimensional Hubbard impurity model. The model has one orbital in the impurity and 11 orbitals in the bath, for a total of 12 sites. This model is possible to calculate with ED, which is plotted for comparison. In Fig. 5.1, we plot the imaginary part of the self-energy for the impurity at various interaction (U) strengths at half-filling and β=400.

It is clear that the RASCI solver is capable of producing excellent quantitative agreement with the ED results for this model at low temperature. This is expected behavior, as RAS-CI has been shown to describe the ground state well, and various truncations of the Hamiltonian are able to

β	U = 2	U = 4	U = 6	U = 8	U = 18
400	4	4	4	4	7
200	14	14	14	14	15

Table 5.1: Number of states m included in the Green's function for 1D Hubbard impurity model, with a cutoff for the Boltzmann factor $e^{-\beta(E_m - E_0)}$ of 10^{-8}. E_0 is the ground state energy.

method	number of determinants
CAS(2,2)CISD	6,044
CISDT	18,819
CISDTQ	98,694
ED	853,776

Table 5.2: Number of determinants required for the 1D Hubbard impurity model.

achieve similar accuracy, but require much fewer determinants than ED. A table displaying this trend for this case is given in Table 5.2. There are only a few excited states that are appreciably occupied and that contribute to the Green's function at this low temperature, as shown in Table 5.1.

Similar to the β=400 case, we obtain excellent quantitative agreement for the imaginary self-energy for the case of β=200, as shown in Fig. 5.2. At β=200, there are more significantly more occupied excited states, as shown in Table 5.1. The RASCI method is capable of describing many low lying excited states for systems at low temperature for this case. These results are obtained with the much cheaper RASCI method, which has polynomial cost, compared with ED, which scales exponentially.

5.4.3 Results for 2D Hubbard Impurity Model

A two dimensional Hubbard model was calculated with the RASCI solver for various interaction strengths and compared with ED results for the imaginary part of the self-energy. Results are plotted in Fig. 5.3. The occupation numbers of these examples show doubly occupied and singly occupied orbitals, requiring the use of a small active space to get a multireference description of the wavefunction. For this reason, we make use of the RAS(2,2)CI method, with the (2,2) indicating that there are two electrons in two orbitals. Unlike the 1D case, we do not see the same level of

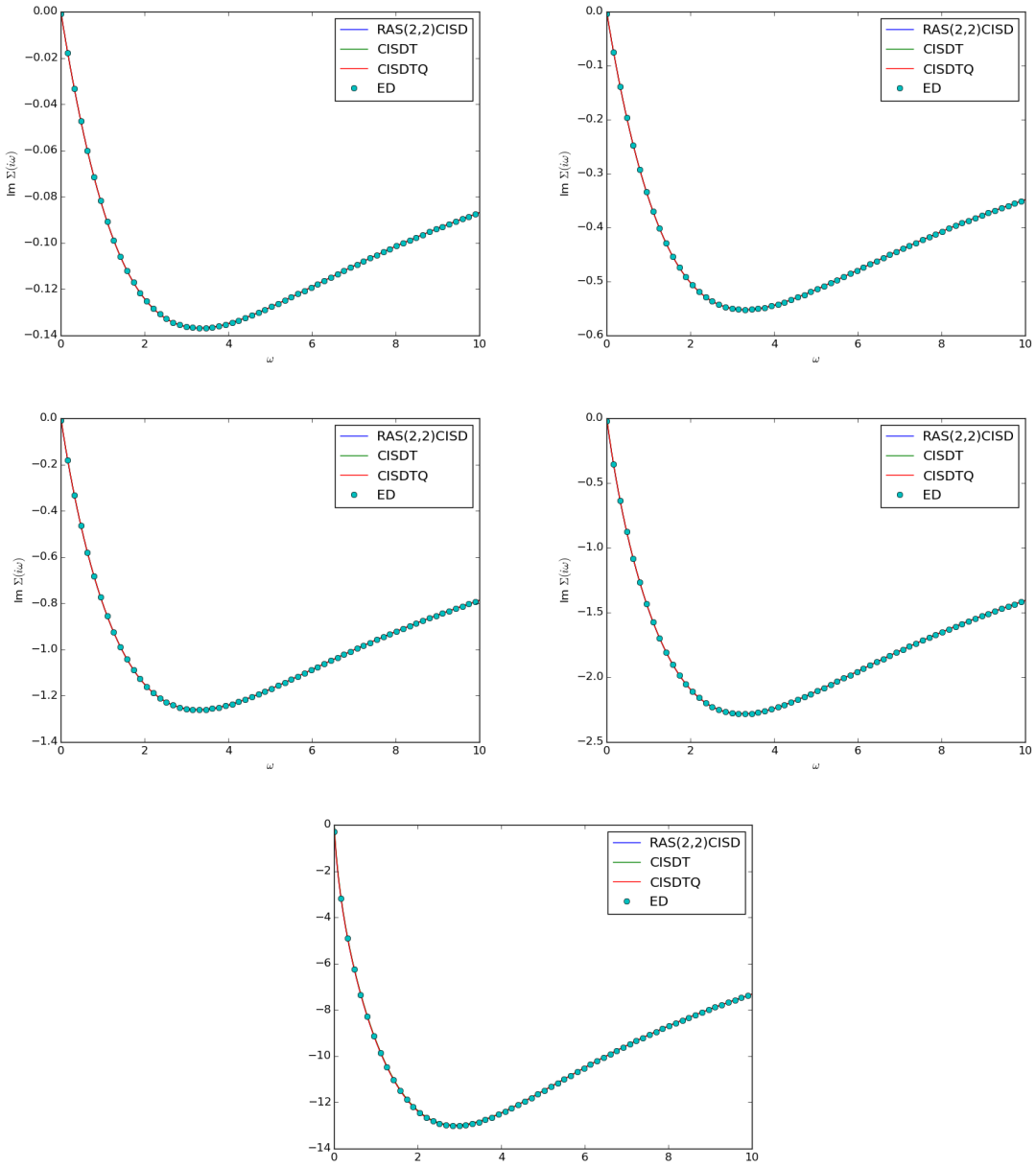

Figure 5.1: 1D Hubbard 12 site impurity with 11 bath orbitals U=2, U=4, U=6, U=8, β=400

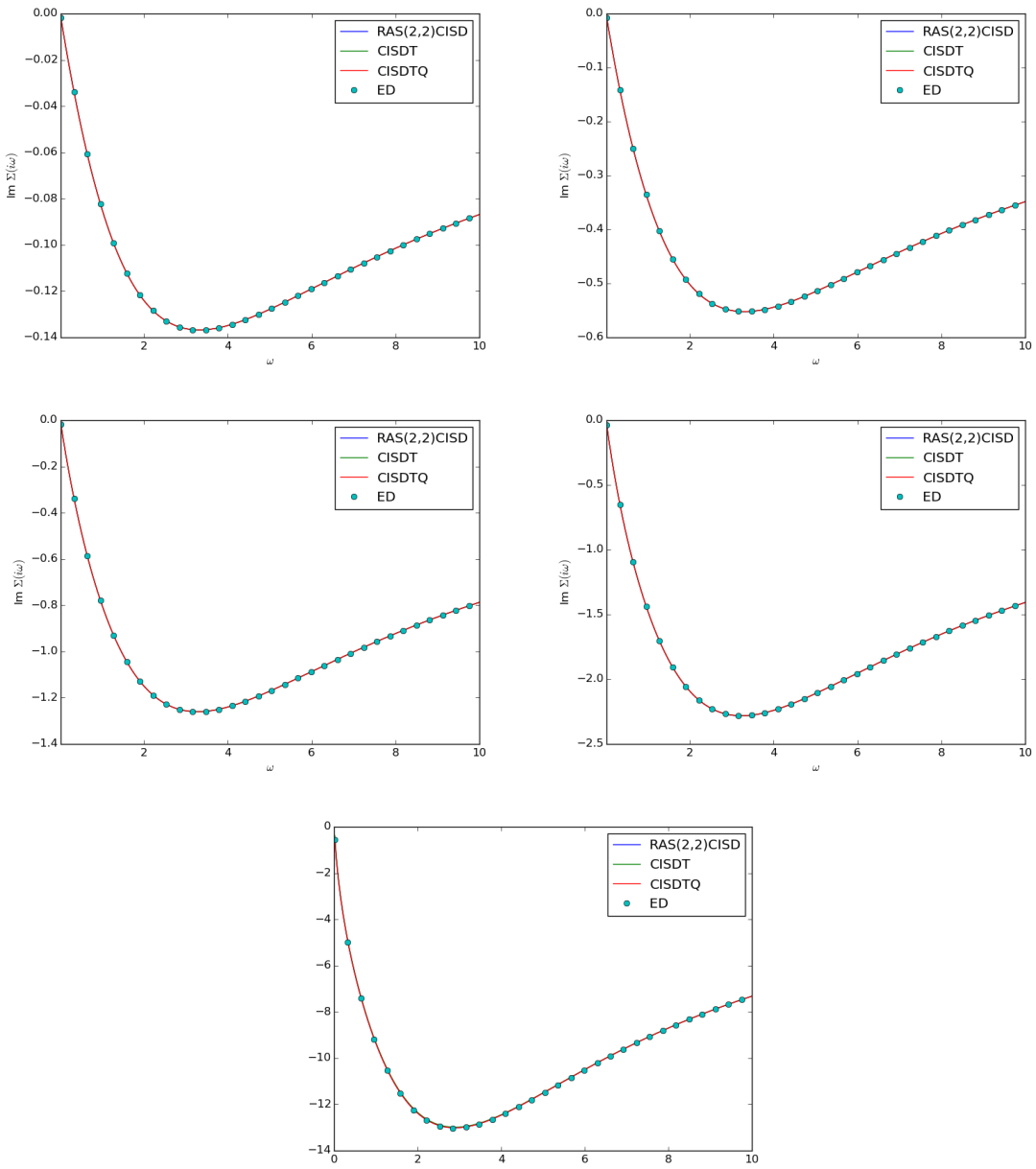

Figure 5.2: 1D Hubbard 12 site impurity with 11 bath orbitals U=2, U=4, U=6, U=8, β=200

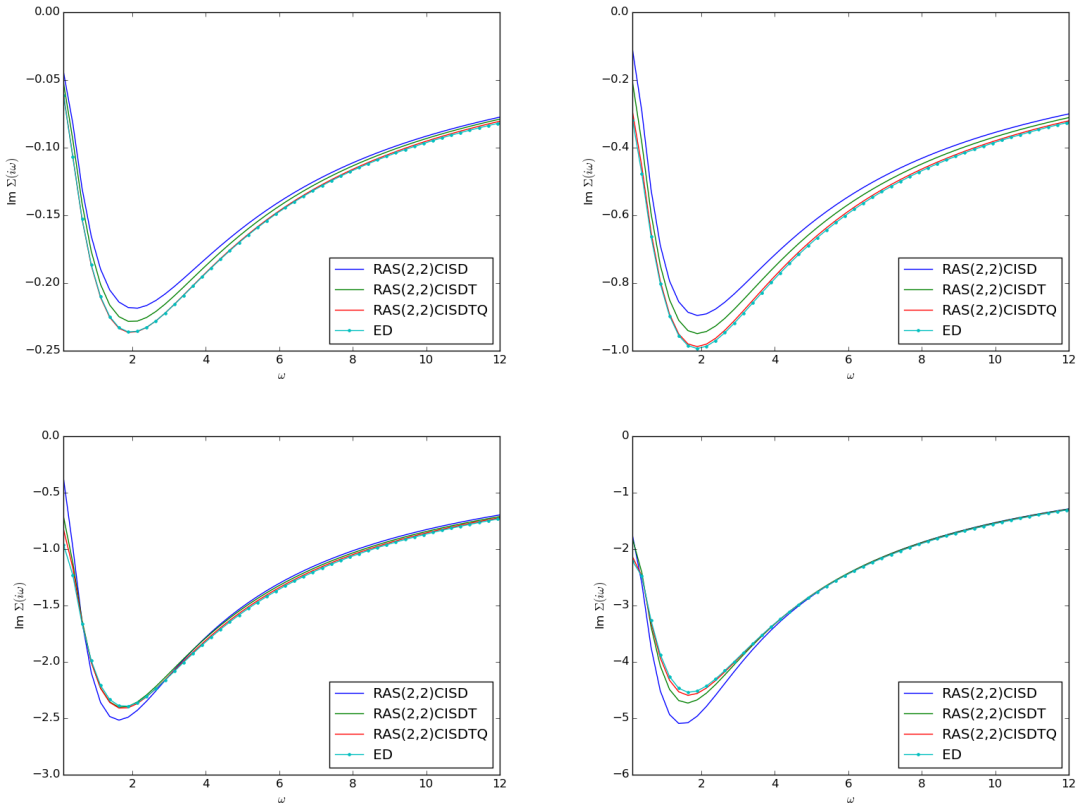

Figure 5.3: 2D Hubbard 4 site impurity with 8 bath orbitals U=2, U=4, U=6, U=8, β=25

quantitative agreement for all levels of CI considered. The results are systematically approaching the ED result as more levels of excitation are included in the CI wavefunction, making the best quantitative agreement with ED from the RAS(2,2)CISDTQ wavefunction.

While this type of RASCI solver has been shown to be capable of producing accurate results for the ground state in the past, we have shown here that we are able to obtain good quantitative agreement when excited states are appreciably occupied. To the best of our knowledge, this is the first temperature dependent RASCI solver to be investigated for low temperatures.

CHAPTER 6

Conclusions

This work has made progress toward understanding the challenges associated with applying finite-temperature Green's functions to study realistic quantum chemical Hamiltonians. The reliability and technical challenges associated with evaluating quantities to directly compare with experiment, including spectra and thermodynamics, were investigated. Additionally, an impurity model in the low temperature regime was implemented for temperature dependent quantum embedding.

In Chapter 3, we have shown that it is possible to evaluate temperature dependent thermodynamic quantities using a self-consistent second-order Green's function method. Using the self-consistent Green's function and self-energy, we were able to evaluate the Luttinger-Ward functional at various temperatures and obtain static thermodynamic quantities such as Helmholtz energy, internal energy, and entropy. Evaluation of these quantities gives us access to the partition function and any thermodynamic quantity that can be derived from it. Unlike the FCI case, in GF2 we do not need to explicitly calculate excited state energies or Boltzmann factors, making calculation of thermodynamic quantities for larger systems feasible.

In Chapter 4, we have investigated the ability of GF2 to calculate IPs, EAs, fundamental gaps, and singlet-triplet gaps for a range of atomic and molecular systems. In general, it was very difficult to obtain EAs in good agreement with UCCSD(T) using any method. There was no method that emerged as the superior method, and results could vary based on the type of system. The most consistent method was building the full self-energy on the real axis, including all of the diagonal elements. This method (F+$\Sigma_{ii}^{(2)}$) was able to give the results similar in accuracy across a range of

systems. Although all quantities computed with the Green's function in this work were done with a second-order evaluation of the self-energy, different evaluation methods can give values for these quantities that differ by several electron volts from each other. This work has reiterated that it is non-trivial to get real axis data from the imaginary axis, and that rigorous investigation of such schemes must be carried out when doing so.

In Chapter 5, we tested a method to construct a temperature-dependent Green's function based on a RASCI formalism. An impurity solver based on restricted active space configuration interaction in a finite-temperature ensemble formalism was implemented and applied to the Hubbard model containing the realistic interactions. Specifically, the solver was benchmarked against ED data for a 1D and 2D Hubbard impurity model. This solver can be used in temperature-dependent embedding schemes such as SEET for systems that are challenging to treat using current solvers. This work can be applied to embedding procedures such as DMFT and SEET for molecules and solid state problems that require the inclusion of temperature-effects. This type of embedding treatment is advantageous for treating larger systems, and additionally for treating systems that contain both strongly and weakly correlated orbitals.

There is still much to be explored in the area of Green's function methods for ab-initio quantum chemistry.

BIBLIOGRAPHY

[1] Kieron Burke and Lucas O Wagner. Dft in a nutshell. *International Journal of Quantum Chemistry*, 113(2):96–101, 2013.

[2] Aurora Pribram-Jones, David A Gross, and Kieron Burke. Dft: A theory full of holes? *Annual review of physical chemistry*, 66:283–304, 2015.

[3] Nicolas Chéron, Denis Jacquemin, and Paul Fleurat-Lessard. A qualitative failure of b3lyp for textbook organic reactions. *Physical Chemistry Chemical Physics*, 14(19):7170–7175, 2012.

[4] Per-Olov Löwdin. Quantum theory of many-particle systems. iii. extension of the hartree-fock scheme to include degenerate systems and correlation effects. *Phys. Rev.*, 97:1509–1520, Mar 1955.

[5] E. Wigner. On the interaction of electrons in metals. *Phys. Rev.*, 46:1002–1011, Dec 1934.

[6] N David Mermin. Thermal properties of the inhomogeneous electron gas. *Physical Review*, 137(5A):A1441, 1965.

[7] MWC Dharma-wardana. Current issues in finite-t density-functional theory and warm-correlated matter. *arXiv preprint arXiv:1602.04734*, 2016.

[8] Vikram Gavini, Kaushik Bhattacharya, and Michael Ortiz. Quasi-continuum orbital-free density-functional theory: A route to multi-million atom non-periodic dft calculation. *Journal of the Mechanics and Physics of Solids*, 55(4):697–718, 2007.

[9] Gianluca Stefanucci and Robert van Leeuwen. *Nonequilibrium Many-Body Theory of Quantum Systems: A Modern Introduction*. Cambridge University Press, 2013.

[10] Richard D Mattuck. *A Guide to Feynman Diagrams in the Many-Body Problem*. Courier Corporation, 2012.

[11] Alexander L Fetter and John Dirk Walecka. *Quantum theory of many-particle systems*. Courier Corporation, 2003.

[12] Alekseĭ Abrikosov. *Methods of quantum field theory in statistical physics*.

[13] Tom Lancaster and Stephen J Blundell. *Quantum field theory for the gifted amateur*. OUP Oxford, 2014.

[14] Takeo Matsubara. A new approach to quantum-statistical mechanics. *Progress of theoretical physics*, 14(4):351–378, 1955.

[15] Antoine Georges and Gabriel Kotliar. Hubbard model in infinite dimensions. *Physical Review B*, 45(12):6479, 1992.

[16] M Jarrell. Hubbard model in infinite dimensions: A quantum monte carlo study. *Physical review letters*, 69(1):168, 1992.

[17] Antoine Georges and Werner Krauth. Numerical solution of the d= hubbard model: Evidence for a mott transition. *Physical review letters*, 69(8):1240, 1992.

[18] Nils Erik Dahlen and Robert van Leeuwen. Self-consistent solution of the dyson equation for atoms and molecules within a conserving approximation. *The Journal of chemical physics*, 122(16):164102, 2005.

[19] Nils Erik Dahlen, Robert van Leeuwen, and Ulf von Barth. Variational energy functionals of the green function and of the density tested on molecules. *Physical Review A*, 73(1):012511, 2006.

[20] Nils Erik Dahlen and Robert van Leeuwen. Solving the kadanoff-baym equations for inhomogeneous systems: application to atoms and molecules. *Physical review letters*, 98(15):153004, 2007.

[21] Donald Allan McQuarrie and John Douglas Simon. *Molecular thermodynamics*. University Science Books Sausalito, CA, 1999.

[22] Joseph W Ochterski. Thermochemistry in gaussian. *Gaussian Inc, Pittsburgh, PA*, pages 1–17, 2000.

[23] Jeff Y. Tsao. *The World of Compound Semiconductors*. Citeseer.

[24] Elio Gabriele Moroni, Göran Grimvall, and Thomas Jarlborg. Free energy contributions to the hcp-bcc transformation in transition metals. *Physical review letters*, 76(15):2758, 1996.

[25] Tang-Qing Yu and Mark E Tuckerman. Temperature-accelerated method for exploring polymorphism in molecular crystals based on free energy. *Physical review letters*, 107(1):015701, 2011.

[26] Qiang Zhu, Alexander G Shtukenberg, Damien J Carter, Tang-Qing Yu, Jingxiang Yang, Ming Chen, Paolo Raiteri, Artem R Oganov, Boaz Pokroy, Iryna Polishchuk, et al. Resorcinol crystallization from the melt: A new ambient phase and new riddles. *Journal of the American Chemical Society*, 138(14):4881–4889, 2016.

[27] N David Mermin. Stability of the thermal hartree-fock approximation. *Annals of Physics*, 21(1):99–121, 1963.

[28] Justin Smith, Aurora Pribram-Jones, and Kieron Burke. Thermal corrections to density functional simulations of warm dense matter. *arXiv preprint arXiv:1509.03097*, 2015.

[29] Valentin V Karasiev, Travis Sjostrom, James Dufty, and SB Trickey. Accurate homogeneous electron gas exchange-correlation free energy for local spin-density calculations. *Physical review letters*, 112(7):076403, 2014.

[30] So Hirata and Xiao He. On the kohn–luttinger conundrum. *The Journal of chemical physics*, 138(20):204112, 2013.

[31] M Altenbokum, K Emrich, H Kümmel, and JG Zabolitzky. A temperature dependent coupled cluster method. In *Condensed matter theories*, pages 389–396. Springer, 1987.

[32] Seikh Hannan Mandal, Rathindranath Ghosh, Goutam Sanyal, and Debashis Mukherjee. A finite-temperature generalisation of the coupled cluster method: A non-perturbative access to grand partition functions. *International Journal of Modern Physics B*, 17(28):5367–5377, 2003.

[33] Matthew R Hermes and So Hirata. Finite-temperature coupled-cluster, many-body perturbation, and restricted and unrestricted hartree–fock study on one-dimensional solids: Luttinger liquids, peierls transitions, and spin-and charge-density waves. *The Journal of Chemical Physics*, 143(10):102818, 2015.

[34] Janez Jaklič and Peter Prelovšek. Lanczos method for the calculation of finite-temperature quantities in correlated systems. *Physical Review B*, 49(7):5065, 1994.

[35] J. Prelovsek, P. Bonca. Ground state and finite temperature lanczos methods. *arXiv preprint arXiv:1111.5931*, 2011.

[36] IE Dzyaloshinski et al. *Methods of quantum field theory in statistical physics*. Courier Corporation, 1975.

[37] Gang Li, Werner Hanke, Alexei N Rubtsov, Sebastian Bäse, and Michael Potthoff. Accessing thermodynamics from dynamical cluster-embedding approaches. *Physical Review B*, 80(19):195118, 2009.

[38] Michael Potthoff, M Aichhorn, and Cristopher Dahnken. Variational cluster approach to correlated electron systems in low dimensions. *Physical Review Letters*, 91(20):206402, 2003.

[39] Michael Potthoff. Self-energy-functional approach: Analytical results and the mott-hubbard transition. *The European Physical Journal B-Condensed Matter and Complex Systems*, 36(3):335–348, 2003.

[40] Michael Potthoff. Making use of self-energy functionals: The variational cluster approximation. *arXiv:1407.4065 [cond-mat.str-el]*.

[41] Michael Potthoff. Self-energy-functional approach to systems of correlated electrons. *The European Physical Journal B-Condensed Matter and Complex Systems*, 32(4):429–436, 2003.

[42] Daniel Neuhauser, Yi Gao, Christopher Arntsen, Cyrus Karshenas, Eran Rabani, and Roi Baer. Breaking the theoretical scaling limit for predicting quasiparticle energies: The stochastic g w approach. *Physical review letters*, 113(7):076402, 2014.

[43] Linda Hung, H Felipe, Jaime Souto-Casares, James R Chelikowsky, Steven G Louie, and Serdar Öğüt. Excitation spectra of aromatic molecules within a real-space g w-bse formalism: Role of self-consistency and vertex corrections. *Physical Review B*, 94(8):085125, 2016.

[44] Mark van Schilfgaarde, Takao Kotani, and S Faleev. Quasiparticle self-consistent g w theory. *Physical review letters*, 96(22):226402, 2006.

[45] Fabio Caruso, Patrick Rinke, Xinguo Ren, Angel Rubio, and Matthias Scheffler. Self-consistent g w: All-electron implementation with localized basis functions. *Physical Review B*, 88(7):075105, 2013.

[46] Sergey V Faleev, Mark Van Schilfgaarde, and Takao Kotani. All-electron self-consistent g w approximation: Application to si, mno, and nio. *Physical review letters*, 93(12):126406, 2004.

[47] Carsten Rostgaard, Karsten Wedel Jacobsen, and Kristian Sommer Thygesen. Fully self-consistent gw calculations for molecules. *Physical Review B*, 81(8):085103, 2010.

[48] Marco Govoni and Giulia Galli. Large scale gw calculations. *Journal of chemical theory and computation*, 11(6):2680–2696, 2015.

[49] Robert van Leeuwen, Nils Erik Dahlen, and Adrian Stan. Total energies from variational functionals of the green function and the renormalized four-point vertex. *Physical Review B*, 74(19):195105, 2006.

[50] Jordan J Phillips and Dominika Zgid. Communication: The description of strong correlation within self-consistent green's function second-order perturbation theory. *The Journal of Chemical Physics*, 140(24):241101, 2014.

[51] Alexander A Rusakov and Dominika Zgid. Self-consistent second-order greens function perturbation theory for periodic systems. *The Journal of chemical physics*, 144(5):054106, 2016.

[52] Alexei A Kananenka, Alicia Rae Welden, Tran Nguyen Lan, Emanuel Gull, and Dominika Zgid. Efficient temperature-dependent green's function methods for realistic systems: using cubic spline interpolation to approximate matsubara green's functions. *Journal of Chemical Theory and Computation*, 2016.

[53] Alexei A Kananenka, Emanuel Gull, and Dominika Zgid. Systematically improvable multiscale solver for correlated electron systems. *Physical Review B*, 91(12):121111, 2015.

[54] Willem Hendrik Dickhoff and Dimitri Van Neck. *Many-body theory exposed!: propagator description of quantum mechanics in many-body systems*. World Scientific, 2008.

[55] Joaquin Mazdak Luttinger and John Clive Ward. Ground-state energy of a many-fermion system. ii. *Physical Review*, 118(5):1417, 1960.

[56] In some texts the functional Φ is simply referred to as the Phi functional and the functional Ω is called the Luttinger-Ward functional.

[57] C-O Almbladh, U Von Barth, and R van Leeuwen. Variational total energies from ϕ-and ψ-derivable theories. *International Journal of Modern Physics B*, 13(05n06):535–541, 1999.

[58] V. Janiš. Stability of self-consistent solutions for the hubbard model at intermediate and strong coupling. *Phys. Rev. B*, 60:11345–11360, Oct 1999.

[59] V Janis. Two-particle renormalizations in many-fermion perturbation theory: the importance of the ward identity. *Journal of Physics: Condensed Matter*, 15(21):L311, 2003.

[60] Jordan J Phillips, Alexei A Kananenka, and Dominika Zgid. Fractional charge and spin errors in self-consistent greens function theory. *The Journal of chemical physics*, 142(19):194108, 2015.

[61] Alexei A Kananenka, Jordan J Phillips, and Dominika Zgid. Efficient temperature-dependent green's functions methods for realistic systems: compact grids for orthogonal polynomial transforms. *Journal of chemical theory and computation*, 2016.

[62] Kristjan Haule Mark van Schilfgaarde Sangkook Choi, Andrey Kutepov and Gabriel Kotliar. First-principles treatment of mott insulators: linearized qsgw+dmft approach. *NPJ Quantum Materials*, 1:16001, 2016.

[63] Gordon Baym and Leo P Kadanoff. Conservation laws and correlation functions. *Physical Review*, 124(2):287, 1961.

[64] Zhuangfei Kou and So Hirata. Finite-temperature full configuration interaction. *Theoretical Chemistry Accounts*, 133(6):1–9, 2014.

[65] In our molecular calculations we have used 200 Legendre polynomials, 50,000 points on the imaginary frequency grid, and 5,200 imaginary-time points, corresponding to the full grid size before the spline interpolation technique was employed for the imaginary frequency grid. One can expect a reduction to 10% of the original grid size using this technique. We used the most strict criteria for the accuracy, corresponding to a $\delta = 10^{-7}$. Additionally, the Legendre basis vastly reduces the cost arising from the number of τ points on the time grid.

[66] Sigeru Huzinaga. *Gaussian basis sets for molecular calculations*. Elsevier, Amsterdam, 1984.

[67] Bela Bauer, LD Carr, Hans G Evertz, Adrian Feiguin, J Freire, S Fuchs, Lukas Gamper, Jan Gukelberger, E Gull, Siegfried Guertler, et al. The alps project release 2.0: open source software for strongly correlated systems. *Journal of Statistical Mechanics: Theory and Experiment*, 2011(05):P05001, 2011.

[68] Pere Miro, Martha Audiffred, and Thomas Heine. An atlas of two-dimensional materials. *Chem. Soc. Rev.*, 43:6537–6554, 2014.

[69] Frank Neese and Edward F Valeev. Revisiting the atomic natural orbital approach for basis sets: Robust systematic basis sets for explicitly correlated and conventional correlated ab initio methods? *Journal of chemical theory and computation*, 7(1):33–43, 2010.

[70] Tran Nguyen Lan, Alexei A Kananenka, and Dominika Zgid. Communication: Towards ab initio self-energy embedding theory in quantum chemistry. *The Journal of chemical physics*, 143(24):241102, 2015.

[71] Tran Nguyen Lan, Alexei A Kananenka, and Dominika Zgid. Rigorous ab initio quantum embedding for quantum chemistry using greens function theory: screened interaction, non-local self-energy relaxation, orbital basis, and chemical accuracy. *Journal of Chemical Theory and Computation*, 2016.

[72] Alexander A Rusakov, Jordan J Phillips, and Dominika Zgid. Local hamiltonians for quantitative green's function embedding methods. *The Journal of chemical physics*, 141(19):194105, 2014.

[73] T Koopmans. Über die zuordnung von wellenfunktionen und eigenwerten zu den einzelnen elektronen eines atoms. *Physica*, 1(1):104 – 113, 1934.

[74] Joseph W Knight, Xiaopeng Wang, Lukas Gallandi, Olga Dolgounitcheva, Xinguo Ren, J Vincent Ortiz, Patrick Rinke, Thomas Körzdörfer, and Noa Marom. Accurate ionization potentials and electron affinities of acceptor molecules iii: A benchmark of gw methods. *Journal of chemical theory and computation*, 2016.

[75] Ryan M Richard, Michael S Marshall, Olga Dolgounitcheva, J Vincent Ortiz, Jean-Luc Bredas, Noa Marom, and C David Sherrill. Accurate ionization potentials and electron affinities of acceptor molecules i. reference data at the ccsd (t) complete basis set limit. *Journal of chemical theory and computation*, 2016.

[76] Lukas Gallandi, Noa Marom, Patrick Rinke, and Thomas Körzdörfer. Accurate ionization potentials and electron affinities of acceptor molecules ii: Non-empirically tuned long-range corrected hybrid functionals. *Journal of chemical theory and computation*, 2016.

[77] Olga Dolgounitcheva, Manuel Diaz-Tinoco, Viatcheslav G Zakrzewski, Ryan M Richard, Noa Marom, C David Sherrill, and J Vincent Ortiz. Accurate ionization potentials and electron affinities of acceptor molecules iv: Electron-propagator methods. *Journal of chemical theory and computation*, 2016.

[78] Jan Linderberg and Yngve Öhrn. *Propagators in quantum chemistry*. John Wiley & Sons, 2004.

[79] D. Van Neck, M. Waroquier, and J. Ryckebusch. Self-consistent solution of the second-order dyson equation for single-particle propagators, with application to the spectral functions of 48ca. *Nuclear Physics A*, 530(2):347 – 369, 1991.

[80] Wei Chen and Alfredo Pasquarello. Band-edge positions in g w: Effects of starting point and self-consistency. *Physical Review B*, 90(16):165133, 2014.

[81] Robert C. Morrison and Paul W. Ayers. Generalized overlap amplitudes using the extended koopmans theorem for be. *J. Chem. Phys.*, 103(15):6556–6561, 1995.

[82] Darwin W. Smith and Orville W. Day. Extension of koopmans' theorem. i. derivation. *The Journal of Chemical Physics*, 62(1):113–114, 1975.

[83] Orville W. Day, Darwin W. Smith, and Robert C. Morrison. Extension of koopmans' theorem. ii. accurate ionization energies from correlated wavefunctions for closed shell atoms. *The Journal of Chemical Physics*, 62(1):115–119, 1975.

[84] Barry T. Pickup. Extended koopmans' theorem and sudden ionization processes. *Chem. Phys. Lett.*, 33(3):422 – 426, 1975.

[85] Robert C. Morrison. The extended koopmans' theorem and its exactness. *J. Chem. Phys.*, 96(5):3718–3722, 1992.

[86] Robert C. Morrison and Guanghua Liu. Extended koopmans' theorem: Approximate ionization energies from mcscf wave functions. *J. Comp. Chem.*, 13(8):1004–1010, 1992.

[87] Jerzy Cioslowski, Pawel Piskorz, and Guanghua Liu. Ionization potentials and electron affinities from the extended koopmans' theorem applied to energy-derivative density matrices: The ektmpn and ektqcisd methods. *The Journal of Chemical Physics*, 107(17):6804–6811, 1997.

[88] Katarzyna Pernal and Jerzy Cioslowski. Ionization potentials from the extended koopmans' theorem applied to density matrix functional theory. *Chem. Phys. Lett.*, 412(13):71 – 75, 2005.

[89] Nils Erik Dahlen and Robert van Leeuwen. Self-consistent solution of the dyson equation for atoms and molecules within a conserving approximation. *J. Chem. Phys.*, 122(16):–, 2005.

[90] Adrian Stan, Nils Erik Dahlen, and Robert van Leeuwen. Levels of self-consistency in the gw approximation. *J. Chem. Phys.*, 130(11):–, 2009.

[91] Uur Bozkaya. The extended koopmans theorem for orbital-optimized methods: Accurate computation of ionization potentials. *The Journal of Chemical Physics*, 139(15):–, 2013.

[92] Fabio Caruso, Matthias Dauth, Michiel J van Setten, and Patrick Rinke. Benchmark of gw approaches for the gw 100 test set. *Journal of chemical theory and computation*, 12(10):5076–5087, 2016.

[93] Carina Faber, Claudio Attaccalite, V. Olevano, E. Runge, and X. Blase. First-principles *GW* calculations for dna and rna nucleobases. *Phys. Rev. B*, 83:115123, Mar 2011.

[94] Marko Schreiber, Mario R Silva-Junior, Stephan PA Sauer, and Walter Thiel. Benchmarks for electronically excited states: Caspt2, cc2, ccsd, and cc3. *The Journal of chemical physics*, 128(13):134110, 2008.

[95] Balazs Hajgató, D Szieberth, P Geerlings, F De Proft, and MS Deleuze. A benchmark theoretical study of the electronic ground state and of the singlet-triplet split of benzene and linear acenes. *The Journal of chemical physics*, 131(22):224321, 2009.

[96] Qiming Sun and Garnet Kin-Lic Chan. Quantum embedding theories. *Accounts of chemical research*, 49(12):2705–2712, 2016.

[97] Dominika Zgid, Emanuel Gull, and Garnet Kin-Lic Chan. Truncated configuration interaction expansions as solvers for correlated quantum impurity models and dynamical mean-field theory. *Physical Review B*, 86(16):165128, 2012.

[98] Attila Szabo and Neil S Ostlund. *Modern quantum chemistry: introduction to advanced electronic structure theory*. Courier Corporation, 2012.

[99] Ronald Hanson, Leo P Kouwenhoven, Jason R Petta, Seigo Tarucha, and Lieven MK Vandersypen. Spins in few-electron quantum dots. *Reviews of Modern Physics*, 79(4):1217, 2007.

[100] Dominika Zgid and Garnet Kin-Lic Chan. Dynamical mean-field theory from a quantum chemical perspective. *The Journal of chemical physics*, 134(9):094115, 2011.

[101] R Brako and D_M Newns. Charge exchange in atom-surface scattering: Thermal versus quantum mechanical non-adiabaticity. *Surface Science*, 108(2):253–270, 1981.